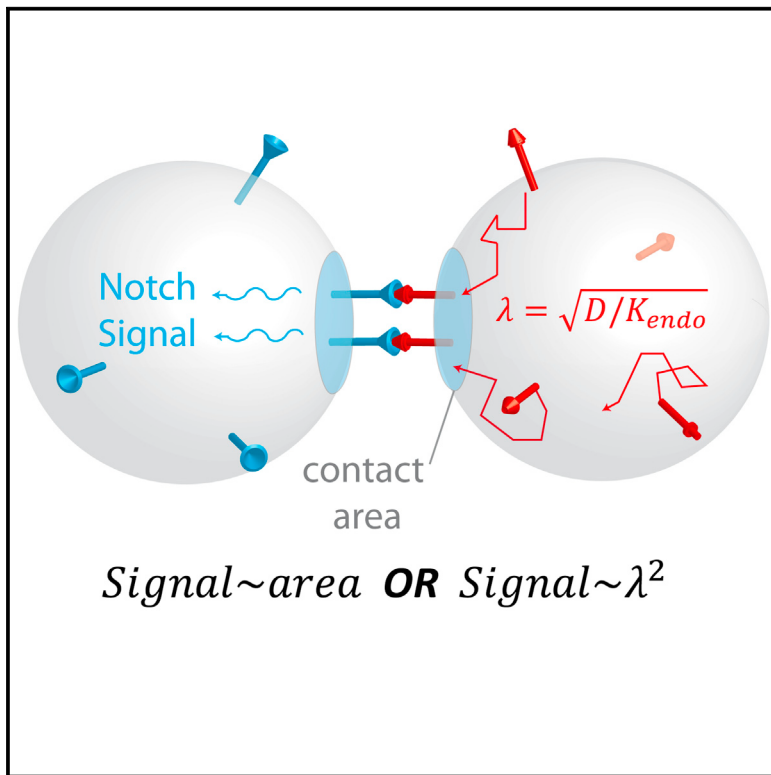


Quantitative Analysis of Delta-like 1 Membrane Dynamics Elucidates the Role of Contact Geometry on Notch Signaling

Graphical Abstract



Authors

Itzhak Khait, Yuval Orsher, Ohad Golan,
Udi Binshtok, Nadav Gordon-Bar,
Liat Amir-Zilberstein, David Sprinzak

Correspondence

davidsp@post.tau.ac.il

In Brief

Khait et al. show large cell-to-cell variability in the diffusion coefficients of the Notch ligand Delta-like 1. A combination of quantitative FRAP-TIRF imaging and mathematical modeling is used to examine the implications of this result on Notch signaling and its dependence on cell-cell contact geometry.

Highlights

- Diffusion coefficients of Dll1 exhibit large cell-to-cell variability
- A model shows how membrane dynamics and contact area affect Notch signaling
- For small contact areas, signal depends on diffusion-length scale of Dll1
- Observed variability can lead to different behaviors in different cellular contexts

Quantitative Analysis of Delta-like 1 Membrane Dynamics Elucidates the Role of Contact Geometry on Notch Signaling

Itzhak Khait,^{1,2} Yuval Orsher,^{1,2} Ohad Golan,¹ Udi Binshtok,¹ Nadav Gordon-Bar,¹ Liat Amir-Zilberstein,¹ and David Sprinzak^{1,*}

¹Department of Biochemistry and Molecular Biology, Wise Faculty of Life Sciences, Tel Aviv University, Tel Aviv 69978, Israel

²Co-first author

*Correspondence: davidsp@post.tau.ac.il

<http://dx.doi.org/10.1016/j.celrep.2015.12.040>

This is an open access article under the CC BY-NC-ND license (<http://creativecommons.org/licenses/by-nc-nd/4.0/>).

SUMMARY

Notch signaling is ubiquitously used to coordinate differentiation between adjacent cells across metazoans. Whereas Notch pathway components have been studied extensively, the effect of membrane distribution and dynamics of Notch receptors and ligands remains poorly understood. It is also unclear how cellular morphology affects these distributions and, ultimately, the signaling between cells. Here, we combine live-cell imaging and mathematical modeling to address these questions. We use a FRAP-TIRF assay to measure the diffusion and endocytosis rates of Delta-like 1 (DII1) in mammalian cells. We find large cell-to-cell variability in the diffusion coefficients of DII1 measured in single cells within the same population. Using a simple reaction-diffusion model, we show how membrane dynamics and cell morphology affect cell-cell signaling. We find that differences in the diffusion coefficients, as observed experimentally, can dramatically affect signaling between cells. Together, these results elucidate how membrane dynamics and cellular geometry can affect cell-cell signaling.

INTRODUCTION

Notch signaling is a highly conserved juxtacrine-signaling pathway, which is repeatedly used for the coordination of differentiation between neighboring cells in metazoans (Artavanis-Tsakonas and Muskavitch, 2010; Artavanis-Tsakonas et al., 1999). Interaction between Notch receptors in one cell, and Notch ligands on a neighboring cell, results in two consecutive proteolytic cleavage events of the Notch receptor (Bray, 2006; Gordon et al., 2008) and the release of its intracellular domain, which then translocates to the nucleus and serves as a co-transcription factor (Nam et al., 2006).

Notch ligand endocytosis is known to be essential for Notch signaling, although its exact role is still controversial (Heuss

et al., 2008; Koo et al., 2005, 2007; Le Borgne, 2006; Weinmaster and Fischer, 2011). It has been suggested that endocytosis and recycling processes are involved in priming of the Notch ligands (Le Borgne, 2006) as well as in exerting a pulling force on the Notch receptors in adjacent cells, required for their activation (Meloty-Kapella et al., 2012; Nichols et al., 2007).

In addition to recycling processes, the membrane distribution of Notch receptors and ligands can be affected by lateral diffusion. Although the role of membrane diffusion has been studied extensively in other signaling pathways (Chung et al., 2010; Jaszkolski and Henley, 2009; Niv et al., 1999; Wang et al., 2008), its role in Notch signaling is still largely unknown (Narui and Salaita, 2013).

The geometry of the contact between cells can also be an important factor affecting Notch signaling. Interestingly, Notch signaling is found to operate in different tissues with very different cell-cell contact morphologies. For example, Notch signaling can be found in adherens junctions where the boundary between cells can extend over several microns (Couturier et al., 2012). In contrast, it has been suggested recently that Notch signaling can be transduced through very thin filopodial contacts between non-adjacent cells (on the order of 0.1–0.2 μm in diameter; Cohen et al., 2010). Such signaling events were shown to be important for proper patterning in bristle spacing in *Drosophila* (Cohen et al., 2010) and in pigment patterning in the zebrafish (Hamada et al., 2014).

How do the lateral diffusion and recycling processes affect the distribution and dynamics of Notch receptors and ligands on the contact between cells? How does the geometry of the contact affect these distributions and ultimately the signaling between cells? Here, we address these questions using a combination of quantitative experiments and mathematical modeling. We performed fluorescence recovery after photobleaching (FRAP) coupled to total internal reflection fluorescence (TIRF) microscopy to measure the diffusion and endocytosis rates of the Notch ligand Delta-like 1 (DII1) in a cell culture assay. We developed a mathematical modeling approach that, together with our experimental results, provides a framework for understanding how the interplay among lateral diffusion, membrane recycling, and geometry of cell contact affects Notch signaling.

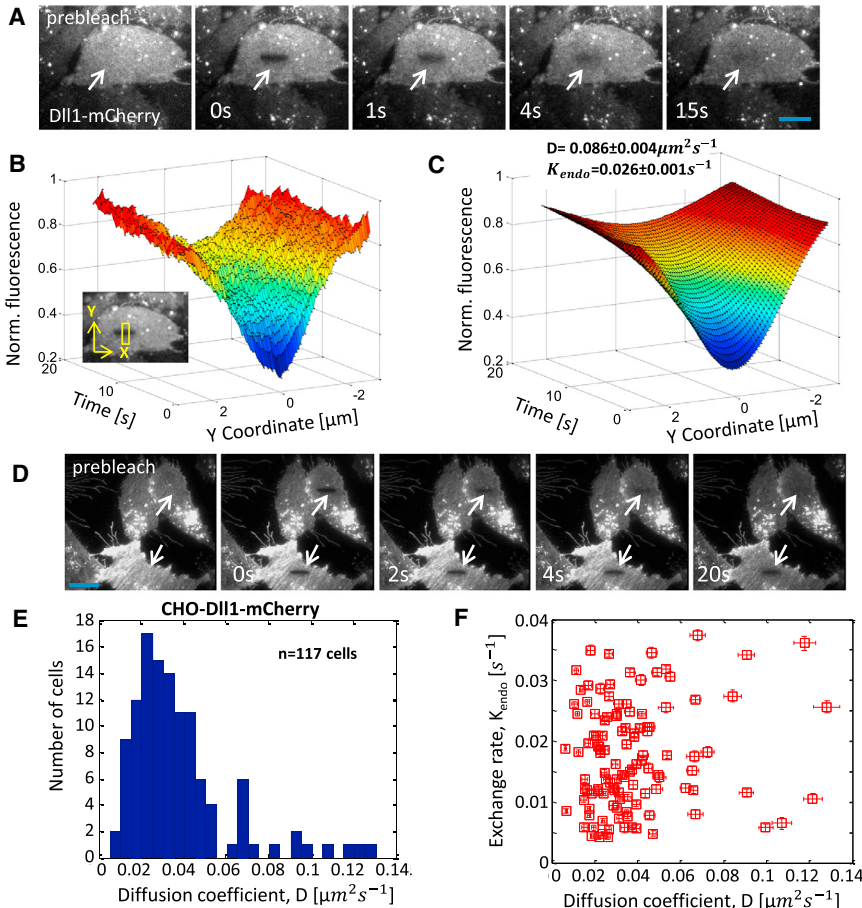


Figure 1. Distribution of Diffusion Coefficients of Dll1 Is Broad

(A) A typical filmstrip from a FRAP-TIRF experiment on CHO-Dll1-mCherry cell (Movie S1). Photobleached region is indicated by arrow. Scale bar (blue), 10 μm .

(B) Shape of fluorescence recovery profile along a rectangle perpendicular to the bleached stripe (y direction in the inset) as a function of time. The fluorescence level at each point is averaged along the axis parallel to the bleached stripe (x direction in the inset). Fluorescence is normalized by the pre-bleach fluorescence level.

(C) A fit of the fluorescence profile shown in (B). The extracted fitting values for this FRAP experiment are $D = 0.086 \pm 0.004 \mu\text{m}^2 \text{s}^{-1}$ and $k_{\text{endo}} = 0.026 \pm 0.001 \text{s}^{-1}$, where the denoted error is the 95% confidence interval on the fitting parameters.

(D) A filmstrip from a FRAP-TIRF experiment on two CHO-Dll1-mCherry cells in parallel (Movie S2). The two cells (arrows) that were photobleached simultaneously exhibit markedly different recovery times. Scale bar (blue), 10 μm .

(E) A histogram of the diffusion coefficients, D , measured in 117 different CHO-Dll1-mCherry cells is shown ($\bar{D} = 0.038 \mu\text{m}^2 \text{s}^{-1}$, $\text{std}(D) = 0.024 \mu\text{m}^2 \text{s}^{-1}$).

(F) Calculated endocytosis rates are uncorrelated with diffusion coefficients values in CHO-Dll1-mCherry cells ($R^2 = 0.11$, $p = 0.24$). Each point in the plot comes from a fit performed on one cell. Error bars shown correspond to the 95% confidence interval on the fitting parameters.

RESULTS

Measuring the Diffusion Coefficient and Endocytosis Rates of Dll1 Using FRAP-TIRF

To understand Notch ligand dynamics, we have developed a method to measure both the lateral diffusion coefficient and the endocytosis rate of Dll1 in mammalian cell culture using FRAP-TIRF (Leake et al., 2006). This method is based on the quantitative analysis of the fluorescence recovery profile in space and time (Goehring et al., 2010). We have applied this method to the Chinese hamster ovary (CHO-K1) cell line that stably expresses rat Dll1 fused to the red fluorescent protein mCherry (Dll1-mCherry) (Sprinzak et al., 2010). Figure 1A shows a filmstrip from a typical FRAP-TIRF experiment on CHO-K1 cells expressing Dll1-mCherry (CHO-Dll1-mCherry). FRAP experiments were performed in regions of the basal membrane in which fluorescence was relatively uniform, avoiding the strongly fluorescent endocytic vesicles observed (Figure 1A; Movie S1). We then analyzed the fluorescence recovery profile (Figure 1B) using a custom image analysis code (see Experimental Procedures) and fitted it to a functional form that takes into account both diffusion and endocytosis (Figure 1C). This allowed us to obtain the effective diffusion coefficient, D , and the endocytosis rate, k_{endo} , for each cell measured (Figure 1C). The values obtained were on the same order of magnitude as previously

measured for other transmembrane proteins (Jacobson et al., 1987; Wiley and Cunningham, 1982).

Diffusion Coefficient of Dll1 Exhibits Broad Cell-to-Cell Distribution

Repeating the same experimental procedure on many CHO-Dll1-mCherry cells, we found that cells exhibit recovery times that are markedly different from each other (Figure 1D; Movie S2). This is despite the fact that all cells originated from a single isogenic clone and were subjected to the same experimental conditions. We found that the distribution of diffusion coefficients is very broad, spanning over more than one order of magnitude, with average $\bar{D} = 0.038 \mu\text{m}^2 \text{s}^{-1}$ and SD of $\text{std}(D) = 0.024 \mu\text{m}^2 \text{s}^{-1}$ (Figure 1E). Similarly, the distribution of endocytosis rates is also quite broad (Figure S1A), with an average of $\bar{k}_{\text{endo}} = 0.018 \text{s}^{-1}$ and SD $\text{std}(k_{\text{endo}}) = 0.009 \text{s}^{-1}$. The endocytosis rates and diffusion coefficients did not show a significant correlation (Figure 1F). The observed variability in diffusion coefficients also was not significantly correlated with the average fluorescence per cell (Figure S1B), although the highest diffusion rates seemed to have lower fluorescence. Similar variability in diffusion and endocytosis rates was observed with Marine Darby canine kidney (MDCK) cells expressing Dll1-mCherry (Figures S1C and S1D), but with significantly higher average values of the diffusion coefficients and endocytosis

rates ($\bar{D} = 0.066 \mu\text{m}^2\text{s}^{-1}$ with $\text{std}(D) = 0.04 \mu\text{m}^2\text{s}^{-1}$ and $\bar{k}_{\text{endo}} = 0.029 \text{ s}^{-1}$ with $\text{std}(k_{\text{endo}}) = 0.019 \text{ s}^{-1}$). We noted that, unlike in CHO-Dll1-mCherry cells, there was a correlation between diffusion and endocytosis rates in MDCK-Dll1-mCherry (Figure S1E). This correlation can potentially arise from the limitation on accurately fitting small endocytosis rates for cells exhibiting higher diffusion rates (Goehring et al., 2010). These results suggest that neither the endocytic recycling nor the expression levels are likely to be responsible for the observed cell-to-cell variability of the diffusion coefficients.

Next, we wanted to check whether cell density or cell cycle can affect the distribution of diffusion coefficients. We therefore performed FRAP-TIRF experiments in three different cell densities. We found that the differences among the distributions in the three different densities were not statistically significant (Figures S1F and S1G). To test whether the cell cycle can affect diffusion rates, we transfected our cells with a Fucci cell-cycle reporter that turns on a green fluorescent marker during the S/G2/M phases (Sakaue-Sawano et al., 2008). We then measured the distribution of diffusion coefficients in the cells expressing the cell-cycle marker. The resulting distribution of diffusion coefficients (Figure S1H) was not significantly different from the general cell population (Figure 1E), suggesting that different membrane dynamics are not related to cell-cycle stage. These measurements indicate that the observed variability is not due to local cell density nor due to cell-cycle stage.

Variability in Different Areas within the Same Cell and between Sister Cells Is Small

To check whether the observed variability is due to differences between cells, we performed FRAP experiments in two areas in the same cell at the same time (Figure 2A; Movie S3). The recovery times for the two areas were typically very similar, and the resulting fitting parameters were highly correlated between the two areas (Figures 2B and S2A). This result suggests that the diffusion coefficients and endocytosis rates are quite uniform within different areas in the same cell and that the observed variability is indeed due to differences between cells. This result also provides evidence that the error in the estimation of diffusion and endocytosis rates is considerably smaller than the observed variability between cells.

We also wanted to determine whether the correlation between diffusion and endocytosis rates persists after cell division. To do that we performed experiments on CHO-Dll1-mCherry cells seeded at low-plating density and imaged after 24 hr (slightly longer than the cell-cycle time of ~20 hrs). We then identified isolated pairs of cells, presumed to be sister cells, and performed FRAP-TIRF experiments on these pairs. We found a significant correlation between the diffusion coefficients of sister cells (Figure 2C) and, to a lesser degree, between the endocytosis rates of sister cells (Figure S2B). This result shows that the timescale associated with changes in diffusion and endocytosis rates is on the order of several hours.

Diffusion of Dll1 in Filopodia Is Faster Than in the Bulk

It has been suggested that Notch signaling between cells can also be transduced through filopodia (Cohen et al., 2010; Hamada et al., 2014). We therefore wanted to test whether Dll1 in filopodia exhibit similar dynamics as Dll1 in the bulk plasma

membrane. We performed FRAP-TIRF experiments on filopodia extending from our CHO-Dll1-mCherry cells (Figure 2D; Movie S4). Although it is known that trafficking along filopodia is controlled by active transport mediated by Myosin X (Mattila and Lappalainen, 2008), we found that the recovery profile in filopodia generally fits a diffusion-like behavior. We used a similar fitting procedure as before to extract the diffusion coefficients within filopodia, with the main difference being that endocytosis was assumed not to contribute in this case. The distribution of effective diffusion coefficients in filopodia was still very broad, with a significantly higher mean ($\bar{D} = 0.06 \mu\text{m}^2\text{s}^{-1}$ with $\text{std}(D) = 0.034 \mu\text{m}^2\text{s}^{-1}$) than in the bulk (Figure 2E). This may indicate that active transport is involved in trafficking of Dll1 in filopodia, enabling faster dynamics than in the bulk.

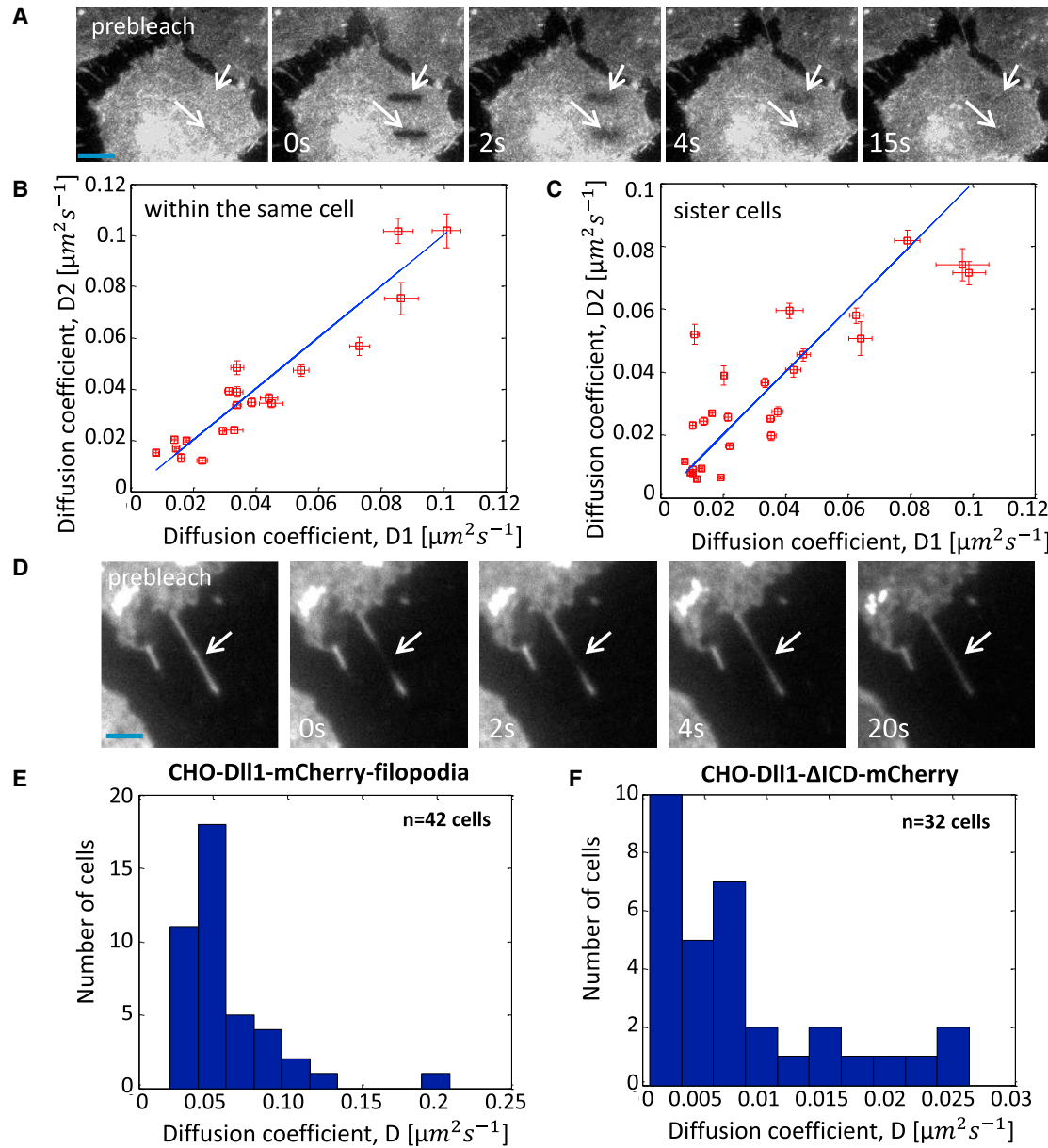
Diffusion Coefficient of Dll1, Lacking the Intracellular Domain, Is Slow

The activity of Dll1 is known to be regulated by ubiquitylation of its intracellular domain by the E3 ubiquitin-ligase Mindbomb1 (Koo et al., 2005, 2007; Lai, 2002; Weinmaster and Fischer, 2011). Dll1 lacking the intracellular domain reaches the membrane but cannot activate Notch receptors in neighboring cells (Heuss et al., 2008; Nichols et al., 2007). To check whether the intracellular domain of Dll1 affects the dynamics on the cell membrane, we generated a stable CHO-K1 cell line expressing Dll1 lacking the intracellular domain and fused to mCherry (CHO-Dll1-ΔICD-mCherry). We found that the distribution of diffusion coefficients of CHO-Dll1-ΔICD-mCherry has a significantly lower average ($\bar{D} = 0.0069 \mu\text{m}^2\text{s}^{-1}$ with $\text{std}(D) = 0.0068 \mu\text{m}^2\text{s}^{-1}$) than the wild-type (Figures 2F and S2C). The distribution of endocytosis rates of CHO-Dll1-ΔICD-mCherry was similar to the corresponding distribution in CHO-Dll1-mCherry (Figure S2D). Also in this cell line, the endocytosis rate did not correlate with the diffusion coefficients (Figure S2E). We noted that the membrane distribution for this mutant was different than the wild-type, showing a more punctate form (Figure S2C). The slower dynamics observed in this mutant suggest that the intracellular domain of Dll1 is necessary for the faster diffusion observed in Figure 1E.

To test whether the observed dynamics of Dll1 are mediated by active transport associated with actin cytoskeleton, we measured how the distribution of diffusion coefficients of CHO-Dll1-mCherry is affected by Latrunculin B (LatB), an inhibitor of actin cytoskeleton. Although the actin cytoskeleton adjacent to the basal membrane was highly affected by LatB (Figure S2F), we found no significant change in the dynamics of Dll1 (Figure S2G). Hence, interaction with actin cytoskeleton is not likely to contribute to variability of Dll1 diffusion coefficients.

Mathematical Model of Notch Delta Signaling

What is the influence of the observed variability in ligand dynamics on developmental processes with different cellular and tissue morphologies? To address this question, we developed a mathematical model that allows us to calculate the dependence of Notch signaling on the dynamics of receptors and ligands as well as on the properties of the contact between cells. We considered a simplified model containing one cell that expresses only Notch receptors and one cell that expresses

**Figure 2. Factors Underlying the Observed Cell-to-Cell Variability in Diffusion Coefficients of Dll1**(A) A filmstrip shows two FRAP experiments on one CHO-Dll1-mCherry cell (Movie S3). Scale bar (blue), 10 μm .(B) Comparison of the diffusion coefficients obtained from two bleached areas within the same CHO-Dll1-mCherry cell (as in A) shows significant correlation ($R^2 = 0.89$, $p < 0.01$). The denoted errors are the 95% confidence interval on the fitting parameters. The blue lines denotes the $D_1 = D_2$ line.(C) Comparison of the diffusion coefficients obtained from two sister cells exhibits significant correlation ($R^2 = 0.85$, $p < 0.01$). The denoted errors are the 95% confidence interval on the fitting parameters. The blue lines denotes the $D_1 = D_2$ line.(D) A filmstrip shows a FRAP-TIRF experiment performed on filopodia extending from a CHO-Dll1-mCherry cell (Movie S4). Scale bar (blue), 10 μm .(E) A histogram of the diffusion coefficients, D , in filopodia, measured in 42 different CHO-Dll1-mCherry cells ($\bar{D} = 0.060 \text{ m}^2\text{s}^{-1}$, $std(D) = 0.034 \mu\text{m}^2\text{s}^{-1}$). This distribution is significantly different from the distribution of diffusion coefficients in the bulk (Figure 1E, $p < 10^{-5}$ as calculated by Wilcoxon rank-sum test).(F) A histogram of the diffusion coefficients, D , measured in 32 different CHO-Dll1-ΔICD-mCherry cells ($\bar{D} = 0.0082 \text{ m}^2\text{s}^{-1}$, $std(D) = 0.0071 \mu\text{m}^2\text{s}^{-1}$). This distribution is significantly different from the distribution of diffusion coefficients in the bulk (Figure 1E, $p < 10^{-10}$ as calculated by Wilcoxon rank-sum test).

only Delta ligands that share a contact with a diameter b (Figures 3A and 3B). We also considered three main processes in our model as follows: (1) Notch receptors and Delta ligands exocytose and endocytose into and out of the cell membrane,

(2) Notch receptors and Delta ligands diffuse laterally on the cell membrane of their respective cells, and (3) Notch receptors and Delta ligands can interact at the contact area. This interaction is described by a simple Michaelis-Menten reaction where a

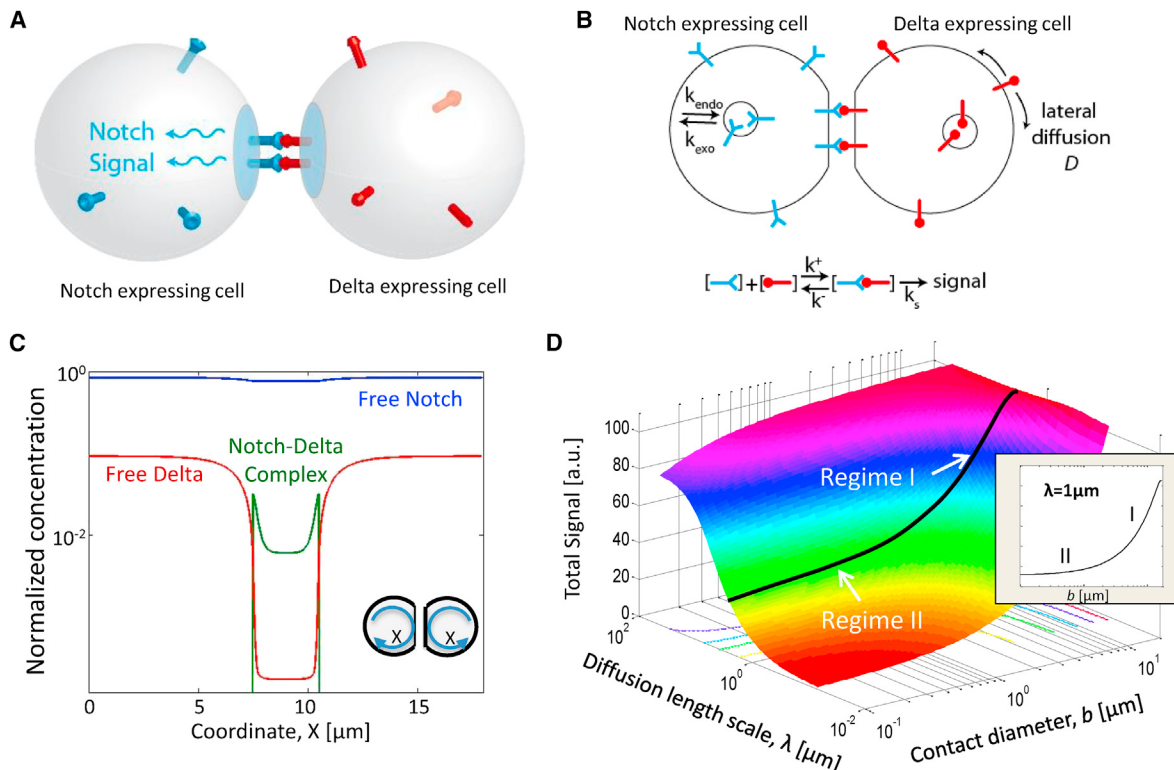


Figure 3. A Mathematical Model of Notch-Delta Signaling Elucidates the Dependence of Notch Signaling on Contact Diameter and Diffusion-Length Scale

- (A) Schematic shows the two-cell model in which a Notch-expressing cell (blue) and a Delta-expressing cell (red) are in direct contact.
- (B) A cross-sectional view of (A) shows the following three processes taken into account in the model: (1) lateral diffusion of Notch and Delta, with diffusion coefficient denoted by D ; (2) endocytosis and exocytosis processes, with rates denoted by K_{endo} and K_{exo} , respectively; and (3) a Michaelis-Menten reaction between Notch and Delta at the boundary described by mass action kinetics (bottom), where k^+ , k^- , and k_s are the on rate, off rate, and catalytic processing rate, respectively.
- (C) Typical steady-state distributions along a cross-section of the cell (see inset) of free Notch (blue), free Delta (red), and the Notch-Delta complex (NDL, green) calculated for a typical parameter set (see parameter estimation in the [Supplemental Experimental Procedures](#)). The concentrations for all variables are normalized by the Notch concentration far from the boundary. Parameter values used are as follows: $k^+ = 0.167 \mu\text{m}^2\text{s}^{-1}$, $k^- = 0.034 \text{s}^{-1}$, $k_s = 0.34 \text{s}^{-1}$, $D = 0.02 \mu\text{m}^2\text{s}^{-1}$, $K_{endo} = 0.02 \text{s}^{-1}$, $D/k_{exo} = 0.2 \mu\text{m}^{-2}\text{s}^{-1}$, $N_0 K_{exo} = 2 \mu\text{m}^{-2}\text{s}^{-1}$, and $b = 3 \mu\text{m}$.
- (D) A plot of the total signal (z axis) as a function of the diffusion-length scale λ (y axis) and the contact diameter b (x axis). The total signal is the integral of the signal density over the contact area. For a fixed value of λ , the total signal exhibits two distinct behaviors as follows (black line and inset): (1) when $b > \lambda$ (regime I), the signal is proportional to the contact area; and (2) when $\lambda > b$, the signal depends very weakly on the contact area. Parameter values used are the same as in (C) except the following: $D = 0.0001 - 36 \mu\text{m}^2\text{s}^{-1}$, $b = 0.1 - 18 \mu\text{m}$.

Notch receptor can bind to a Delta ligand at the boundary, forming a Notch-Delta complex. This complex is then processed to generate the signal, which in our case is the concentration of cleaved Notch intracellular domain (NICD) produced in the cell (Sprinzak et al., 2010; Figure 3B; see [Experimental Procedures](#) for details).

Using these processes, we derived a set of reaction-diffusion equations that describe the dynamics of the membrane concentrations of free Notch, free Delta, and the Notch-Delta complex. Steady-state distributions of free Notch, free Delta, and the Notch-Delta complex along the perimeter of the two cells are shown in Figure 3C for a typical set of parameters. Although we considered the case of more Notch than Delta in this example, the opposite case of more Delta than Notch shows a similar behavior with Notch and Delta switching roles (Figure S3A; [Experimental Procedures](#)).

Diffusion and Endocytosis Rates Determine the Concentration Profiles of Notch and Delta

Our model shows that the distribution of free Delta exhibits a dip at the contact area between cells (red curve in Figure 3C), reflecting the fact that in this area free Delta is quickly captured by the abundant free Notch in the neighboring cell. Free Notch levels also decrease but to a much lesser extent, since only a small fraction of the free Notch is captured by Delta (blue curve in Figure 3C). Notch-Delta complexes accumulate at the boundary and are restricted to it (green curve in Figure 3C).

Diffusion tends to broaden the steady-state concentration profile of free Delta (Figure S3B). The broadening of the free Delta concentration profile is determined by the diffusion-length scale of free Delta, $\lambda = \sqrt{D/k_{endo}}$, where D and k_{endo} are the diffusion coefficient and endocytosis rate of Delta, respectively. The diffusion-length scale describes the typical distance a Delta protein

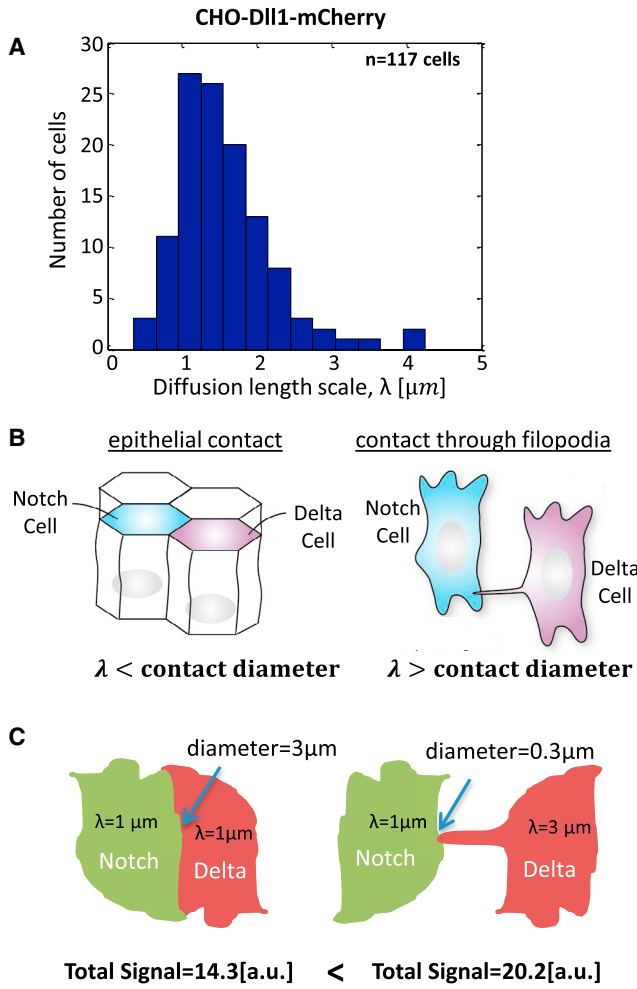


Figure 4. Diffusion-Length Scale of Dll1 Is Variable and Is on the Same Order of Magnitude as Typical Contact Diameters

(A) A histogram showing the distribution of diffusion-length scales, λ , for CHO-Dll1-mCherry measured in 117 different cells. The distribution is quite broad, with mean $\lambda = 1.56 \mu\text{m}$ and SD of $0.64 \mu\text{m}$ (same cells as Figure 1E).

(B) Implications of the results in different tissue morphologies. For epithelial contacts, the typical contact diameter is expected to be larger than the average diffusion-length scale measured in (A), corresponding to regime I in Figure 3D. For contact through filopodia, the contact diameter may be smaller than the average diffusion-length scale measured in (A), corresponding to regime II in Figure 3D.

(C) Two scenarios for Notch signaling between pairs of cells with different contact diameters. Assuming values obtained in (A), the signal through a small contact area (right pair, total signal = 20.2) can be higher than the signal through a large contact area (left pair, total signal = 14.3), depending on the respective diffusion-length scales in the two pairs. Parameter values used are the same as in Figure 3C except the following: $D^N = 0.02 \mu\text{m}^2\text{s}^{-1}$, $D^{D1} = 0.09, 0.02 \mu\text{m}^2\text{s}^{-1}$, $K_{endo}^N = 0.02 \text{s}^{-1}$, $K_{endo}^{D1} = 0.01, 0.02 \text{s}^{-1}$, $b = 0.3, 3 \mu\text{m}$.

diffuses on the cell membrane before it endocytoses. Hence, the contact area serves as a sink; free Delta flows into it from a region determined by the diffusion-length scale, λ . We noted that the diffusion of the Notch-Delta complex has almost no effect on the distributions of free Notch and free Delta (Figure S3C). A detailed analysis of the dependence of the concentration pro-

files on the parameters of the model is provided in the [Supplemental Experimental Procedures](#) (Figures S3D and S3E).

Signaling Depends on Diffusion-Length Scale and Contact Area

Next, we asked how the two relevant length scales of the system, the diffusion-length scale, λ , and the diameter of the contact area, b , affect the signal in the Notch-expressing cell (Figure 3D). Interestingly, calculation of the dependence of the signal on these two length scales in our model revealed two distinct regimes as follows: (1) if the contact diameter is larger than the diffusion-length scale (i.e., $b > \lambda$), then the diffusion has only a small contribution to the signal and the signal would be proportional to the contact area between cells; and (2) if the contact diameter is smaller than the diffusion-length scale (i.e., $b < \lambda$), then the signal is dominated by the influx of Delta ligands into the contact area and, therefore, has only weak dependence on the diameter of the contact area. In this regime, the signal is due to ligands that come from an effective area of λ^2 , which is much bigger than the contact area. Faster ligand diffusion can strongly affect signaling between cells in this regime. Hence, our results suggest that the dependence of Notch signaling on the size of the contact area crucially depends on the typical diffusion-length scales of Notch and Delta.

Measured Diffusion-Length Scale of Dll1 Is Variable and Is on the Same Order of Magnitude as Typical Contact Diameters

Given that our FRAP-TIRF measurements provided both the diffusion coefficient, D , and the endocytosis rate, K_{endo} , of Dll1, we could calculate the diffusion-length scale of Dll1 in each of the cells measured in Figure 1E. Figure 4A shows the distribution of λ for CHO-Dll1-mCherry cells. We found that the average diffusion-length scale was $\lambda = 1.56 \mu\text{m}$ with SD of $0.64 \mu\text{m}$. Similar values are obtained for the diffusion-length scale of MDCK-Dll1-mCherry (Figure S4A). Interestingly, the measured values of λ showed that, depending on contact morphology, the diffusion-length scale can be either smaller (epithelial contacts) or larger (filopodia) than the cell-cell contact diameter (Figure 4B). It is interesting to note that the diffusion-length scale of the mutant Dll1-ΔICD-mCherry was about three times smaller than that of the wild-type Dll1 (Figure S4B), reflecting the slower membrane dynamics of the mutant (Figure 2F).

DISCUSSION

This work focuses on the question of how and when Notch ligand dynamics on the plasma membrane affect Notch signaling between cells. By using a quantitative analysis of FRAP-TIRF on live cells (rather than looking at fixed samples), we were able to obtain both the diffusion coefficients and endocytosis rates of Dll1 in single mammalian cells. Our measurements reveal large cell-to-cell variability in both diffusion coefficients and endocytosis rates (Figures 1E and S1A).

Why do different cells in the same monoclonal population exhibit different diffusion coefficients of Dll1? We found that the observed distribution of diffusion coefficients has weak or no correlation with the endocytosis rate and with the level of expression

of Dll1 (Figures 1F, S1B, and S1E). We show that cell density, cell cycle, and inhibition of actin cytoskeleton do not significantly affect the distributions of diffusion coefficients and endocytosis rates (Figures S1F–S1H and S3E). We also show that variability in different areas within the same cell is much smaller than cell-to-cell variability (Figure 2B), suggesting that the diffusion and endocytosis rates are cell-intrinsic properties. These cellular properties are maintained for relatively long timescales, on the order of hours, since we found correlations between the diffusion coefficients and endocytosis rates in sister cells (Figures 2C and S2B).

Recent evidence on Notch signaling through filopodia (Cohen et al., 2010; Hamada et al., 2014) also prompted us to test whether the dynamics of Dll1 trafficking in filopodia are significantly different than that in the bulk plasma membrane. We found that the distribution of effective diffusion coefficients in filopodia also exhibits large cell-to-cell variability, but on average has significantly higher effective diffusion than that in the bulk (Figures 2D and 2E). It is known that active retrograde and anterograde trafficking contributes to transport in filopodia (Mattila and Lappalainen, 2008). Hence, the observed faster dynamics of Dll1 trafficking along filopodia is potentially due to such active transport.

Given that the activity of Dll1 is regulated by ubiquitylation of its intracellular domain (Le Borgne, 2006; Weinmaster and Fischer, 2011), we also tested the dynamics of Dll1 lacking its intracellular domain. Our findings show that the mutant Dll1-ΔICD exhibits significantly slower dynamics than the wild-type form (Figures 2F and S4B). This result suggests a potential new function for the Dll1 intracellular domain: controlling the effective diffusion coefficient and, hence, ligand dynamics. It will be interesting to check whether this regulation of ligand dynamics is also mediated by ubiquitylation.

To understand how the observed dynamics affect signaling between cells, we developed a mathematical modeling approach that elucidates the interplay between membrane dynamics and cell morphology. The results of the model emphasize the importance of the diffusion-length scale of the Notch ligand λ . This length scale directly depends on the diffusion coefficients and the endocytosis rates we measured. Our model suggests that signaling between cells exhibits a qualitatively different behavior depending on the value of λ . If the contact diameter between cells is larger than the diffusion-length scale ($b > \lambda$), then the signal is proportional to the contact area (regime I in Figure 3D). On the other hand, if the contact diameter is smaller than the diffusion-length scale ($b < \lambda$), then the signal depends very weakly on the contact area and instead is controlled by the influx of ligands (or receptors) from the area surrounding the contact region (regime II in Figure 3D). Experimentally, we found that the diffusion-length scales of Dll1 are in the range of 0.58–4.17 μm (Figure 4A), which is on the same order of magnitude as the typical contact diameters between cells (Farhadifar et al., 2007; Puliafito et al., 2012).

These results have implications on the way Notch signaling operates in different tissue morphologies. Tissues containing cellular morphologies with large contact diameters, such as epithelial morphology (left in Figure 4B), are expected to be in regime I ($b > \lambda$). In such tissues, lateral diffusion should play only a minor role in signaling and the signal will be proportional to the contact area. In contrast, in filopodia, which have very small contact diam-

eters (on the order of 0.1–0.3 μm ; Mattila and Lappalainen, 2008), we expect to be in regime II ($b < \lambda$) (right in Figure 4B). Thus, the signal through filopodia is determined mainly by the diffusion of ligands (or receptors) into the contact area rather than by ligands already present at the contact area. The magnitude of signaling in this case should be independent of the contact diameter.

The observed broad distribution in the diffusion coefficients of Dll1 leads to a broad distribution of the diffusion-length scales (Figure 4A). This broad distribution implies that cells may actively control cell-to-cell signaling by regulating the diffusion-length scale. To illustrate this point, we considered the hypothetical situation shown in Figure 4C, where two pairs of Notch-Delta cells with very different contact diameters are compared (assuming 3- μm diameter for the left pair and 0.3- μm diameter for the right pair). If all other parameters were equal, clearly the signal going through the pair with the larger contact would be higher. However, if we assume that the diffusion length of Delta is higher in the pair with smaller contact (3 μm in the right pair versus 1 μm in the left pair), then our model predicts that the signal through that pair would be higher (Figure 4C), even though its contact area is two orders of magnitude smaller. This example shows that differences in the diffusion-length scales, as observed experimentally, may strongly affect the ability of cells to communicate. Furthermore, it shows that Notch signaling between cells can, in principle, be regulated by actively controlling the diffusion-length scale of membrane ligands (or receptors).

EXPERIMENTAL PROCEDURES

Description of Genetic Constructs and Cell Lines

The Dll1-mCherry fusion construct was developed previously (Sprinzak et al., 2010). The Dll1-ΔICD-mCherry construct was constructed using Gibson cloning (Gibson et al., 2009) based on the pcDNA5-TO-Dll1-mCherry vector (Sprinzak et al., 2010), where the intracellular domain was deleted from position 561 (Valine) to 714 (Valine) (Meloty-Kapella et al., 2012). The generation of stable CHO-Dll1-mCherry cells was described previously (Sprinzak et al., 2010). Stable CHO-Dll1-ΔICD-mCherry and MDCK-Dll1-mCherry cells were generated using the same procedure (Sprinzak et al., 2010).

Description of Experimental Protocols and Microscopy

Cells were plated 72 hr prior to imaging, in low, medium, and high densities (25,000, 50,000, and 100,000 cells, respectively), on a glass-bottom 30-mm plate (SPL Lifesciences), in growth medium (α MEM) containing 100 ng/ml doxycycline (Sigma). Prior to imaging, media were replaced with low-fluorescence imaging media (Sprinzak et al., 2010).

Microscopy Details

Cells were imaged in FRAP-TIRF Till photonics system (described in Grunwald et al., 2013). Photobleaching was performed on a $0.5^{\circ}7 \mu\text{m}^2$ bleach area with 100% power of the 561-nm laser for a total bleach time of 40 ms. Two images were taken before the bleach and 70 images were taken every 0.35 s.

Image Analysis

We used a semi-automatic analysis code (MATLAB 8.0, MathWorks) for data extraction and fitting procedure. Full details of the image analysis and the fitting procedures are provided in the *Supplemental Experimental Procedures*. In brief, we defined for each movie a region of interest around the bleached area. The fluorescence profile as a function of time was extracted, corrected for background level and photobleaching, and averaged along the axis parallel to the bleached stripe, resulting in a one-dimensional (1D) fluorescence profile for each time point (as in Figure 1C).

For the experiments testing cell-cycle dependence (Figure S1H), CHO-Dll1-mCherry cells were transiently transfected with the cell-cycle reporter Fucci-S/G2/M (Amalgaam) 36 hr prior to imaging. FRAP-TIRF measurements

were performed only on cells expressing high levels of the Fucci marker. For the experiments with cytoskeleton inhibitor (**Figures S2F** and **S2G**), cells were incubated with 0.2 μM LatB (Sigma) or DMSO in control for 2 hr prior to imaging. To verify inhibition by LatB, Dll1-mCherry cells were transiently transfected with EGFP-lifeAct (a kind gift from Benny Shilo) 24 hr prior to imaging (**Figure S2F**).

Fitting Procedure

The fitting procedure was adapted from [Goehring et al. \(2010\)](#). In brief, we used the following fitting function:

$$A \left\{ 1 - \frac{f_b}{2} e^{-K_{endo} t} \left[\operatorname{erf} \left(m \frac{\frac{d_y}{2} - y}{\sqrt{4Dm^2 t + 1}} \right) + \operatorname{erf} \left(m \frac{\frac{d_y}{2} + y}{\sqrt{4Dm^2 t + 1}} \right) \right] \right\}$$

We first fit the first post-bleach image to the function at $t = 0$. This provides values for A , the steady-state fluorescence far from the bleach center; d_y , the extent of the bleach region; m , the steepness of the boundaries of the bleach area; and f_b , the fraction that was bleached. We then used these values to fit all the profiles in the movie and obtain the diffusion coefficient D and the endocytosis rate K_{endo} . A similar fitting procedure was performed on filopodia (**Figure 3A**), but with K_{endo} taken to be zero (no endocytosis in filopodia).

To assess significance of the correlations in **Figures 1F**, **2B**, **2C**, **S1B**, **S1E**, **S2A**, **S2B**, and **S2E**, we calculated the Pearson correlations and the associated p values for obtaining such correlations. To assess the significance of the difference between the distributions in **Figures 2E**, **2F**, **S1C**, **S1F**, and **S1G** and that of wild-type Dll1-mCherry in **Figure 1E**, we used the Wilcoxon rank-sum test.

Mathematical Model

We considered a simplified geometry in which the two cells are described by large two-dimensional (2D) disks, with a contact area with diameter b at the center. We took into account three main processes as follows: (1) Notch receptors (N) and Delta ligands (Dl) exocytose into the cell membrane, in their respective cells, from a large cytoplasmic pool (N_0 and Dl_0 , assumed to be constant) with rates $k_{exo}^N N_0$ and $k_{exo}^{Dl} Dl_0$, respectively; Notch receptors and Delta ligands also endocytose back into the cytoplasmic pool with rates k_{endo}^N and k_{endo}^{Dl} , respectively; (2) Notch receptors and Delta ligands diffuse laterally on the cell membrane of their respective cells with diffusion constants of D^N and D^{Dl} ; and (3) Notch receptors and Delta ligands can interact at the contact area. This interaction is described by a simple Michaelis-Menten reaction where a Notch receptor on one cell can bind to a Delta ligand at the boundary, forming a Notch-Delta complex ($[NDl]$), with association and dissociation rates k^+ and k^- . The Notch-Delta complex can be processed at a rate k_s to generate the signal S , which in our case is the intracellular domain of Notch ([Sprinzak et al., 2010](#); **Figure 3B**).

Our model includes four reaction diffusion equations for the concentrations of Notch receptor, Delta ligand, Notch-Delta complex, and the total signal, respectively, as follows:

$$\frac{dN}{dt} = D_N \nabla^2 N + k_{exo}^N N_0 - k_{endo}^N N + I_b(r)(k^- [NDl] - k^+ NDl) \quad (\text{Equation 1})$$

$$\frac{dDl}{dt} = D_{Dl} \nabla^2 Dl + k_{exo}^{Dl} Dl_0 - k_{endo}^{Dl} Dl + I_b(r)(k^- [NDl] - k^+ NDl) \quad (\text{Equation 2})$$

$$\frac{d[NDl]}{dt} = I_b(r)(D_{[NDl]} \nabla^2 [NDl] + k^+ NDl - k^- [NDl] - k_s [NDl]) \quad (\text{Equation 3})$$

$$\frac{dS}{dt} = I_b(r)k_s \int [NDl] d^2r - \gamma S \quad (\text{Equation 4})$$

Where γ is the degradation rate of the signal S , and $I_b(r)$ is the Heavyside theta function defined as follows:

$$I_b(r) = \begin{cases} 1 & \text{for } r \leq b \\ 0 & \text{elsewhere} \end{cases} \quad (\text{Equation 5})$$

The total signal is obtained by integrating the signal concentration over the contact area (Equation 4). We assume that the diffusion coefficient of the Notch-Delta complex $[NDl]$ is $D_{[NDl]} = (D_{Dl} + D_N)/4$.

The diffusion in Equations 1, 2, and 3 is a 2D diffusion. Since the problem is radially symmetric, we could reduce the dimensionality of the equations by switching to polar coordinates. For details see the [Supplemental Experimental Procedures](#).

SUPPLEMENTAL INFORMATION

Supplemental Information includes Supplemental Experimental Procedures, four figures, one table, and four movies and can be found with this article online at <http://dx.doi.org/10.1016/j.celrep.2015.12.040>.

AUTHOR CONTRIBUTIONS

Conceptualization, D.S. and I.K.; Methodology, D.S., I.K., and Y.O.; Investigation, I.K., Y.O., O.G., U.B., and N.G.-B.; Writing – Original Draft, D.S. and I.K.; Writing – Review & Editing, D.S., I.K., and Y.O.; Resources, L.A.-Z.

ACKNOWLEDGMENTS

We acknowledge Sheila Weinreb for help with the experiments and Oren Shaya, Micha Hersch, Iftach Nachman, and Avigdor Eldar for critically reviewing the manuscript. We thank Benny Shilo for kindly providing the EGFP-lifeAct construct. We thank Uri Ashery and Irit Gottfried for help with the FRAP-TIRF system. This work was supported by grants from the Israeli Science Foundation (grant 1021/11) and a Marie Curie European Reintegration Grant.

Received: August 5, 2015

Revised: October 26, 2015

Accepted: December 6, 2015

Published: December 31, 2015

REFERENCES

- Artavanis-Tsakonas, S., and Muskavitch, M.A. (2010). Notch: the past, the present, and the future. *Curr. Top. Dev. Biol.* 92, 1–29.
- Artavanis-Tsakonas, S., Rand, M.D., and Lake, R.J. (1999). Notch signaling: cell fate control and signal integration in development. *Science* 284, 770–776.
- Bray, S.J. (2006). Notch signalling: a simple pathway becomes complex. *Nat. Rev. Mol. Cell Biol.* 7, 678–689.
- Chung, I., Akita, R., Vandlen, R., Toomre, D., Schlessinger, J., and Mellman, I. (2010). Spatial control of EGF receptor activation by reversible dimerization on living cells. *Nature* 464, 783–787.
- Cohen, M., Georgiou, M., Stevenson, N.L., Miodownik, M., and Baum, B. (2010). Dynamic filopodia transmit intermittent Delta-Notch signaling to drive pattern refinement during lateral inhibition. *Dev. Cell* 19, 78–89.
- Couturier, L., Vodovar, N., and Schweigert, F. (2012). Endocytosis by Numb breaks Notch symmetry at cytokinesis. *Nat. Cell Biol.* 14, 131–139.
- Farhadifar, R., Röper, J.C., Aligouy, B., Eaton, S., and Jülicher, F. (2007). The influence of cell mechanics, cell-cell interactions, and proliferation on epithelial packing. *Curr. Biol.* 17, 2095–2104.
- Gibson, D.G., Young, L., Chuang, R.Y., Venter, J.C., Hutchison, C.A., 3rd, and Smith, H.O. (2009). Enzymatic assembly of DNA molecules up to several hundred kilobases. *Nat. Methods* 6, 343–345.
- Goehring, N.W., Chowdhury, D., Hyman, A.A., and Grill, S.W. (2010). FRAP analysis of membrane-associated proteins: lateral diffusion and membrane-cytoplasmic exchange. *Biophys. J.* 99, 2443–2452.
- Gordon, W.R., Arnett, K.L., and Blacklow, S.C. (2008). The molecular logic of Notch signaling—a structural and biochemical perspective. *J. Cell Sci.* 121, 3109–3119.
- Grunwald, A., Gottfried, I., Cox, A.D., Haklai, R., Kloog, Y., and Ashery, U. (2013). Rasosomes originate from the Golgi to dispense Ras signals. *Cell Death Dis.* 4, e496.

- Hamada, H., Watanabe, M., Lau, H.E., Nishida, T., Hasegawa, T., Parichy, D.M., and Kondo, S. (2014). Involvement of Delta/Notch signaling in zebrafish adult pigment stripe patterning. *Development* 141, 318–324.
- Heuss, S.F., Ndiaye-Lobry, D., Six, E.M., Israël, A., and Logeat, F. (2008). The intracellular region of Notch ligands DLL1 and DLL3 regulates their trafficking and signaling activity. *Proc. Natl. Acad. Sci. USA* 105, 11212–11217.
- Jacobson, K., Ishihara, A., and Inman, R. (1987). Lateral diffusion of proteins in membranes. *Annu. Rev. Physiol.* 49, 163–175.
- Jaskolski, F., and Henley, J.M. (2009). Synaptic receptor trafficking: the lateral point of view. *Neuroscience* 158, 19–24.
- Koo, B.K., Lim, H.S., Song, R., Yoon, M.J., Yoon, K.J., Moon, J.S., Kim, Y.W., Kwon, M.C., Yoo, K.W., Kong, M.P., et al. (2005). Mind bomb 1 is essential for generating functional Notch ligands to activate Notch. *Development* 132, 3459–3470.
- Koo, B.K., Yoon, M.J., Yoon, K.J., Im, S.K., Kim, Y.Y., Kim, C.H., Suh, P.G., Jan, Y.N., and Kong, Y.Y. (2007). An obligatory role of mind bomb-1 in notch signaling of mammalian development. *PLoS ONE* 2, e1221.
- Lai, E.C. (2002). Protein degradation: four E3s for the notch pathway. *Curr. Biol.* 12, R74–R78.
- Le Borgne, R. (2006). Regulation of Notch signalling by endocytosis and endosomal sorting. *Curr. Opin. Cell Biol.* 18, 213–222.
- Leake, M.C., Chandler, J.H., Wadhams, G.H., Bai, F., Berry, R.M., and Armitage, J.P. (2006). Stoichiometry and turnover in single, functioning membrane protein complexes. *Nature* 443, 355–358.
- Mattila, P.K., and Lappalainen, P. (2008). Filopodia: molecular architecture and cellular functions. *Nat. Rev. Mol. Cell Biol.* 9, 446–454.
- Meloty-Kapella, L., Shergill, B., Kuon, J., Botvinick, E., and Weinmaster, G. (2012). Notch ligand endocytosis generates mechanical pulling force dependent on dynamin, epsins, and actin. *Dev. Cell* 22, 1299–1312.
- Nam, Y., Sliz, P., Song, L., Aster, J.C., and Blacklow, S.C. (2006). Structural basis for cooperativity in recruitment of MAML coactivators to Notch transcription complexes. *Cell* 124, 973–983.
- Narui, Y., and Salaita, K. (2013). Membrane tethered delta activates notch and reveals a role for spatio-mechanical regulation of the signaling pathway. *Bioophys. J.* 105, 2655–2665.
- Nichols, J.T., Miyamoto, A., Olsen, S.L., D'Souza, B., Yao, C., and Weinmaster, G. (2007). DSL ligand endocytosis physically dissociates Notch1 heterodimers before activating proteolysis can occur. *J. Cell Biol.* 176, 445–458.
- Niv, H., Gutman, O., Henis, Y.I., and Kloog, Y. (1999). Membrane interactions of a constitutively active GFP-Ki-Ras 4B and their role in signaling. Evidence from lateral mobility studies. *J. Biol. Chem.* 274, 1606–1613.
- Puliafito, A., Hufnagel, L., Neveu, P., Streichan, S., Sigal, A., Fygenson, D.K., and Shraiman, B.I. (2012). Collective and single cell behavior in epithelial contact inhibition. *Proc. Natl. Acad. Sci. USA* 109, 739–744.
- Sakaue-Sawano, A., Kurokawa, H., Morimura, T., Hanyu, A., Hama, H., Osawa, H., Kashiwagi, S., Fukami, K., Miyata, T., Miyoshi, H., et al. (2008). Visualizing spatiotemporal dynamics of multicellular cell-cycle progression. *Cell* 132, 487–498.
- Sprinzak, D., Lakhanpal, A., Lebon, L., Santat, L.A., Fontes, M.E., Anderson, G.A., Garcia-Ojalvo, J., and Elowitz, M.B. (2010). Cis-interactions between Notch and Delta generate mutually exclusive signalling states. *Nature* 465, 86–90.
- Wang, Q., Zhang, X., Zhang, L., He, F., Zhang, G., Jamrich, M., and Wensel, T.G. (2008). Activation-dependent hindrance of photoreceptor G protein diffusion by lipid microdomains. *J. Biol. Chem.* 283, 30015–30024.
- Weinmaster, G., and Fischer, J.A. (2011). Notch ligand ubiquitylation: what is it good for? *Dev. Cell* 21, 134–144.
- Wiley, H.S., and Cunningham, D.D. (1982). The endocytic rate constant. A cellular parameter for quantitating receptor-mediated endocytosis. *J. Biol. Chem.* 257, 4222–4229.

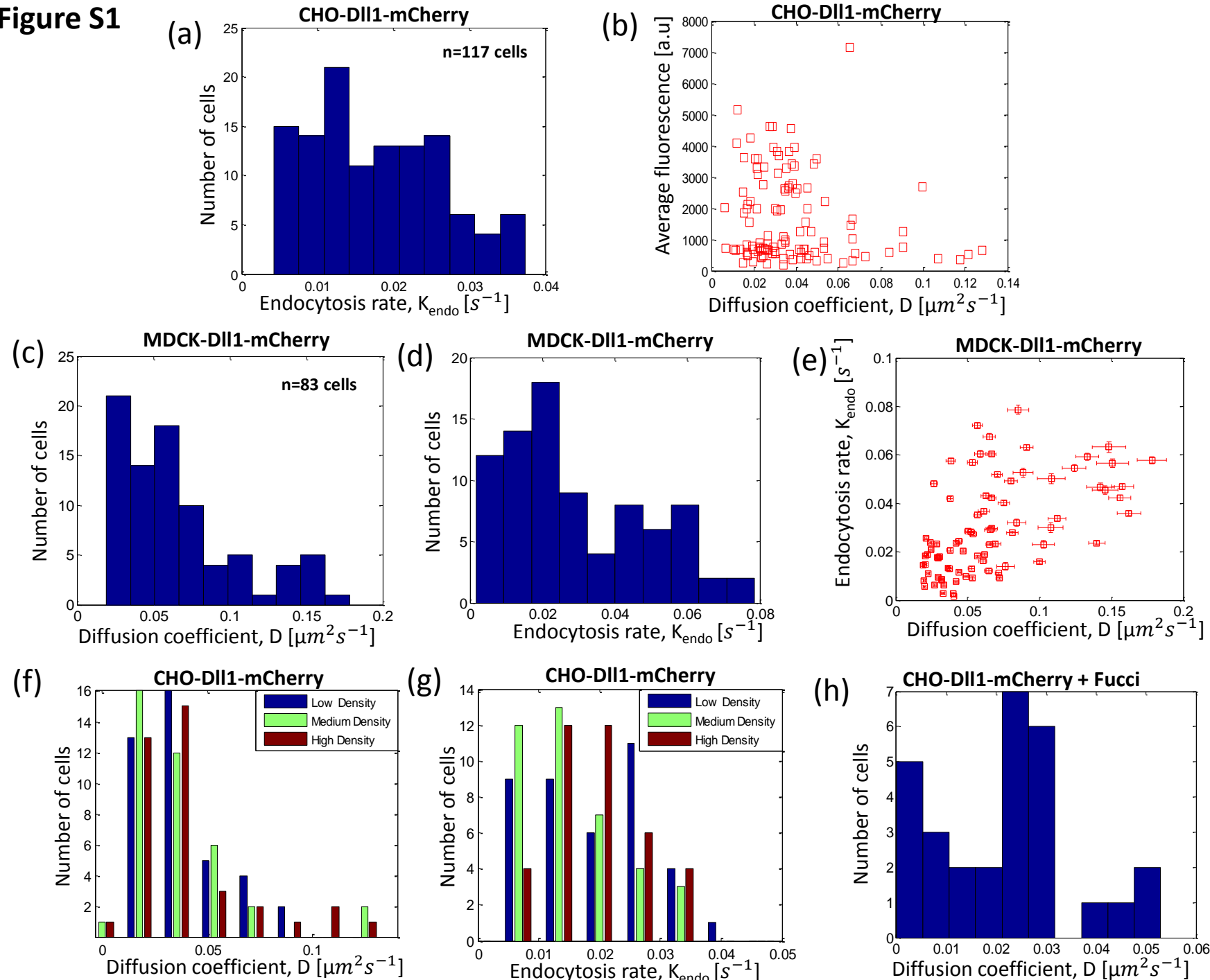
Figure S1

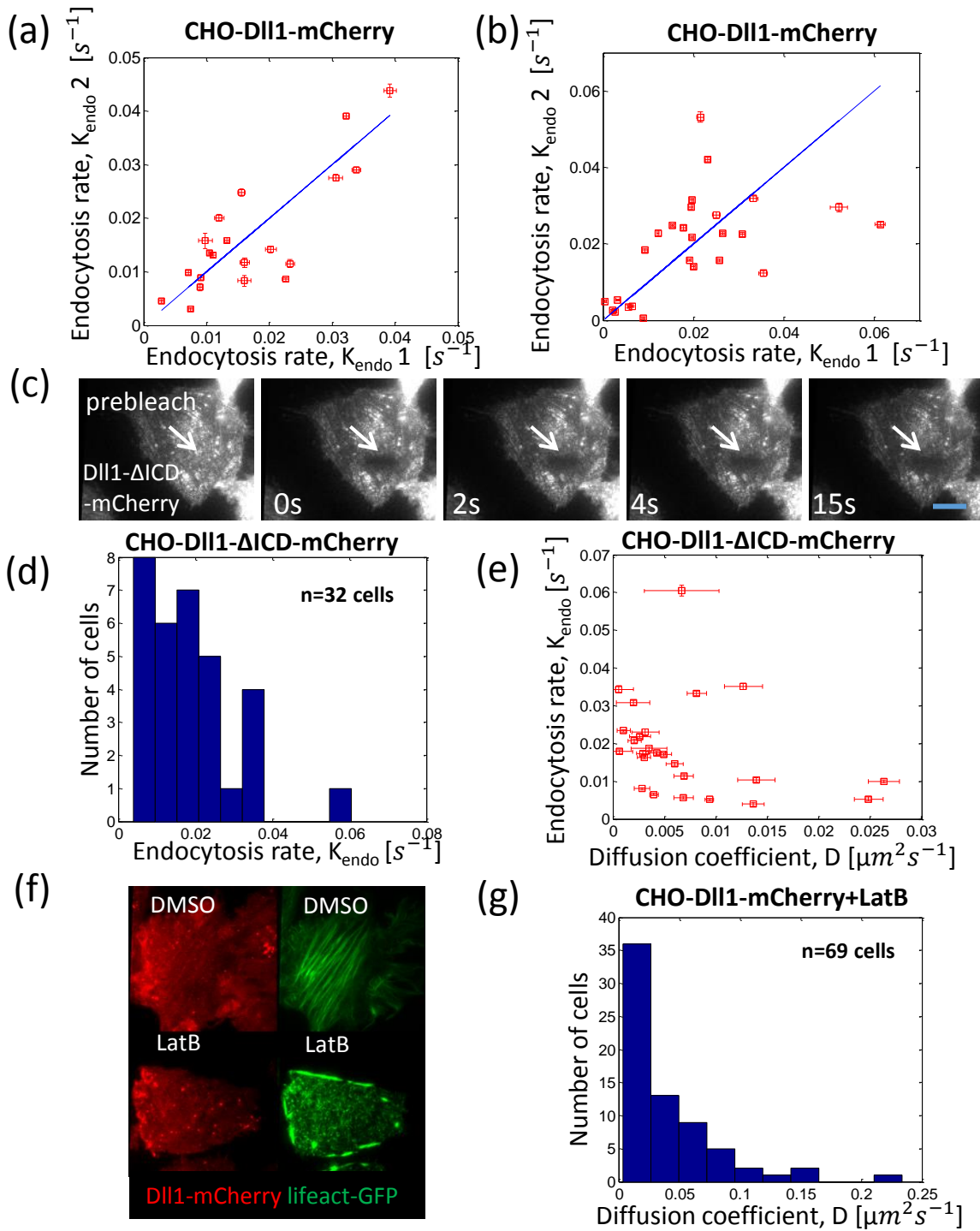
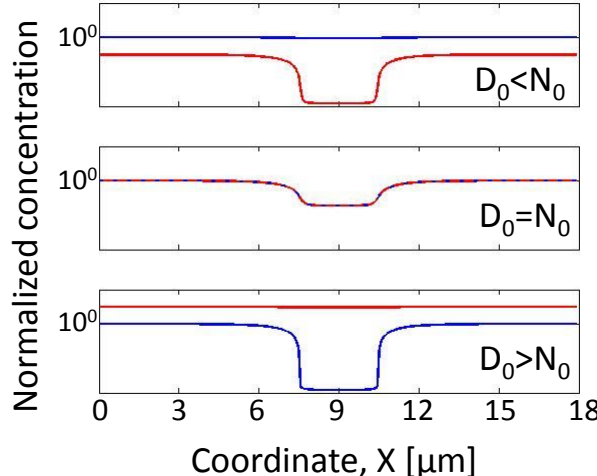
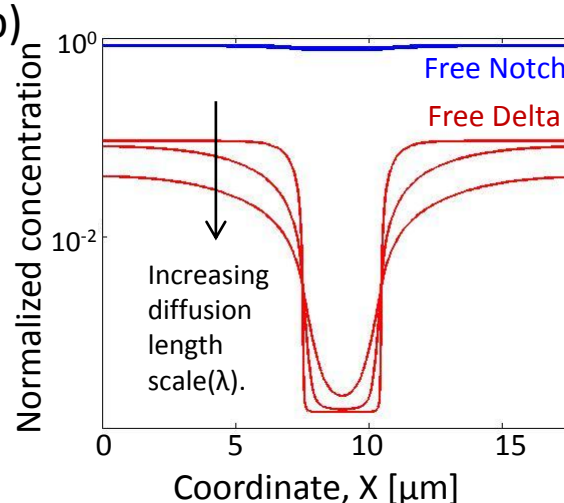
Figure S2

Figure S3

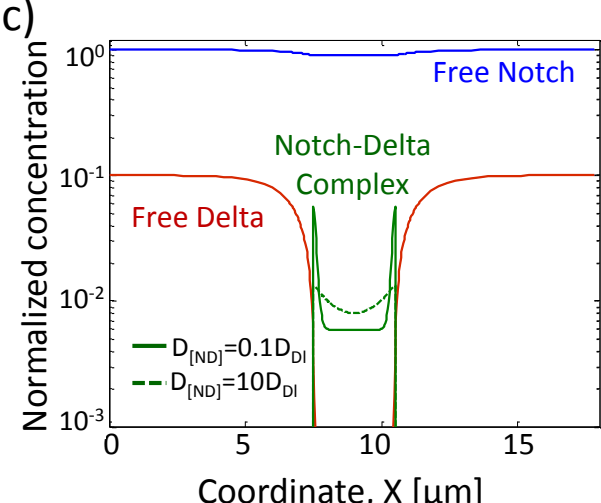
(a)



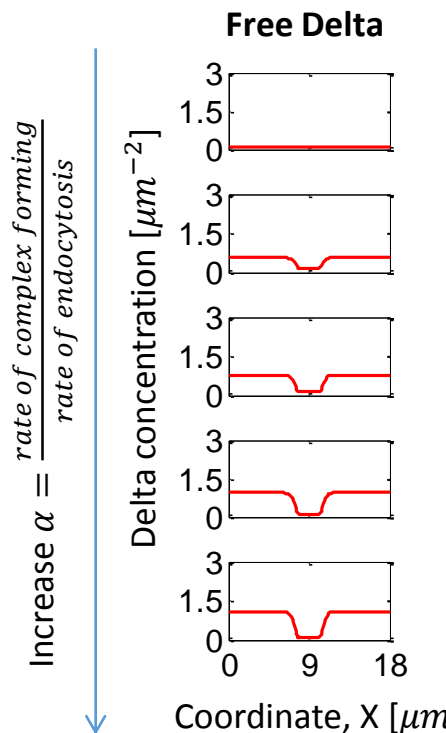
(b)



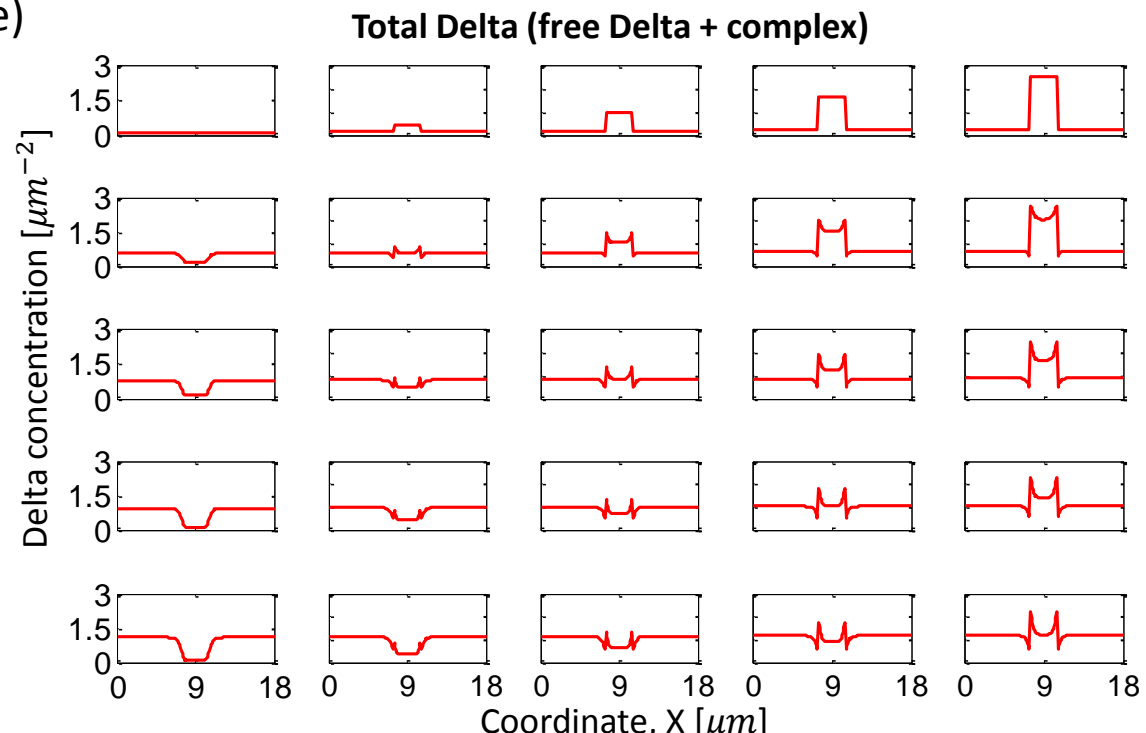
(c)



(d)



(e)



$$\text{Increase } \beta = \frac{\text{rate of complex forming}}{\text{rate of complex processing}}$$

Figure S4

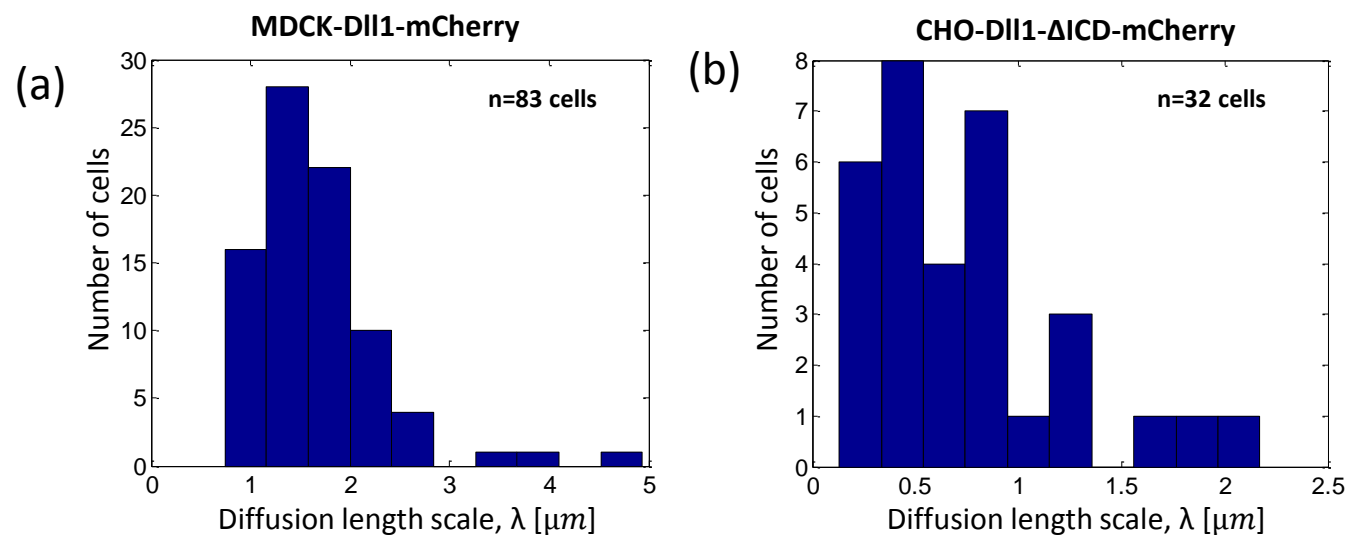


Table S1

Figure	Parameters
3c	$k^+ = 0.167 \mu m^2 s^{-1}$, $k^- = 0.034 s^{-1}$, $k_S = 0.34 s^{-1}$, $D = 0.02 \mu m^2 s^{-1}$, $K_{endo} = 0.02 s^{-1}$, $Dl_0 K_{exo} = 0.2 \mu m^{-2} s^{-1}$, $N_0 K_{exo} = 2 \mu m^{-2} s^{-1}$, $b = 3 \mu m$
3d	$k^+ = 0.167 \mu m^2 s^{-1}$, $k^- = 0.034 s^{-1}$, $k_S = 0.34 s^{-1}$, $D = 0.0001 - 36 \mu m^2 s^{-1}$, $K_{endo} = 0.02 s^{-1}$, $Dl_0 K_{exo} = 0.2 \mu m^{-2} s^{-1}$, $N_0 K_{exo} = 2 \mu m^{-2} s^{-1}$, $b = 0.1 - 18 \mu m$
4c	$k^+ = 0.167 \mu m^2 s^{-1}$, $k^- = 0.034 s^{-1}$, $k_S = 0.34 s^{-1}$, $D^N = 0.02 \mu m^2 s^{-1}$, $D^{Dl} = 0.09, 0.02 \mu m^2 s^{-1}$, $k_{endo}^N = 0.02 s^{-1}$, $k_{endo}^{Dl} = 0.01, 0.02 s^{-1}$, $0.2 \mu m^{-2} s^{-1}$, $N_0 K_{exo} = 2 \mu m^{-2} s^{-1}$, $b = 0.3, 3 \mu m$
S3a	$k^+ = 0.167 \mu m^2 s^{-1}$, $k^- = 0.034 s^{-1}$, $k_S = 0.34 s^{-1}$, $D = 0.02 \mu m^2 s^{-1}$, $K_{endo} = 0.02 s^{-1}$, $Dl_0 K_{exo} = 0.2, 2, 20 \mu m^{-2} s^{-1}$, $N_0 K_{exo} = 2 \mu m^{-2} s^{-1}$, $b = 3 \mu m$
S3b	$k^+ = 0.167 \mu m^2 s^{-1}$, $k^- = 0.034 s^{-1}$, $k_S = 0.34 s^{-1}$, $D = 0.005, 0.16, 1 \mu m^2 s^{-1}$, $K_{endo} = 0.02 s^{-1}$, $Dl_0 K_{exo} = 0.2 \mu m^{-2} s^{-1}$, $N_0 K_{exo} = 2 \mu m^{-2} s^{-1}$, $b = 3 \mu m$
S3c	$k^+ = 0.167 \mu m^2 s^{-1}$, $k^- = 0.034 s^{-1}$, $k_S = 0.34 s^{-1}$, $D = 0.02 \mu m^2 s^{-1}$, $K_{endo} = 0.02 s^{-1}$, $Dl_0 K_{exo} = 0.2 \mu m^{-2} s^{-1}$, $N_0 K_{exo} = 2 \mu m^{-2} s^{-1}$, $b = 3 \mu m$, $D_{[NDI]} = 0.002, 0.2 \mu m^2 s^{-1}$
S3d,e	$k^+ = 0.167 \mu m^2 s^{-1}$, $k^- = 0.034 s^{-1}$, $D = 0.02 \mu m^2 s^{-1}$, $Dl_0 K_{exo} = 0.2 \mu m^{-2} s^{-1}$, $N_0 K_{exo} = 2 \mu m^{-2} s^{-1}$, $b = 3 \mu m$, $\alpha = \frac{k^+ N_{ss}}{K_{endo}}$, $= 0.10, 2.57, 5.05, 7.52, 10.00 [a.u.]$, $\beta = \frac{k^+ N_{ss}}{k^- + k_S} = 0.10, 2.57, 5.05, 7.52, 10.00 [a.u.]$

Supplemental Information

Supplemental Figure Captions

Figure S1. Broad distributions of endocytosis rates and diffusion coefficients of Dll1 are observed in different cell lines and different conditions. Related to Fig. 1 (a) A histogram showing the distribution of endocytosis rates, K_{endo} , of CHO-Dll1-mCherry cells measured in 117 different cells. The average endocytosis rate is $K_{endo} = 0.018\text{s}^{-1}$ with standard deviation of 0.009s^{-1} . (b) Diffusion coefficients of CHO-Dll1-mCherry cells are uncorrelated with the average fluorescence in the cells ($R^2=-0.124$, $p=0.18$). Each point in the plot comes from a fit performed on one cell. Average fluorescence was measured by averaging on the pre-bleached area. Error bars shown correspond to the 95% confidence interval on the fitting parameters. (c) A histogram showing the distribution of diffusion coefficients, D , of MDCK-Dll1-mCherry cells measured in 83 different cells. The average diffusion coefficients is $D = 0.066\mu\text{m}^2\text{s}^{-1}$ with standard deviation of $0.04\mu\text{m}^2\text{s}^{-1}$. This distribution is significantly different from the distribution of diffusion coefficients in the bulk (Fig. 1e, $p<10^{-8}$ as calculated by Wilcoxon rank-sum test) (d) A histogram showing the distribution of endocytosis rates, K_{endo} , of MDCK-Dll1-mCherry cells measured in 83 different cells. The average endocytosis rate is $K_{endo} = 0.029\text{s}^{-1}$ with standard deviation of 0.019s^{-1} . (e) Calculated K_{endo} exhibit significant correlation with diffusion coefficients values in MDCK-Dll1-mCherry cells ($R^2=0.54$, $p<0.01$). Each point in the plot comes from a fit performed on one cell. The observed correlation reflects the fact that in this cell line we observe high Diffusion coefficients making it harder to estimate endocytosis rates (Goehring et al., 2010). Error bars shown correspond to the 95% confidence interval on the fitting parameters. (f) The distribution of diffusion coefficients was measured in CHO-Dll1-mCherry cells plated in three different cell densities. Here low, medium, and high densities correspond to 25,000, 50,000, and 100,000 cells per 35mm plate, respectively. The distributions in the different densities are not significantly different ($p_{lm}=0.55$, $p_{lh}=0.92$, $p_{mh}=0.69$ as calculated by Wilcoxon rank-sum test). (g) The distribution of endocytosis rates for the same cells as in (a). The distributions in the different densities are marginally significant or not significantly different ($p_{lm}=0.08$, $p_{lh}=0.81$, $p_{mh}=0.04$ as calculated by Wilcoxon rank-sum test). Since the low and high densities are clearly similar we associate the observed difference in the medium density as a statistical outlier. (h) The distribution of diffusion coefficients was measured in CHO-Dll1-mCherry cells transfected with Fucci cell cycle reporter that turns on a green fluorescent marker during the S/G2/M phases. FRAP-TIRF experiments were performed only on cells expressing green fluorescence

indicating they are in the S/G2/M phase. The distribution of diffusion coefficients is not significantly different than the distribution of the full cell population in Fig. 1e ($p=0.114$ as calculated by Wilcoxon rank-sum test).

Figure S2. Factors affecting diffusion coefficients and endocytosis rates of Dll1. Related to Fig. 2 (a) Comparison of the endocytosis rates obtained from two bleached areas within the same CHO-Dll1-mCherry cell (as in 2(e)). The denoted errors correspond to the 95% confidence interval on the fitting parameters. These results show that the endocytosis rates estimated for the two bleached stripes are significantly correlated (close to the $K_{endo}1 = K_{endo}2$ line (blue), $R^2=0.6712$, $p=0.0014$). (b) Comparison of the endocytosis rates obtained from two sister cells (as in 2(f)). The denoted errors correspond to the 95% confidence interval on the fitting parameters. These results show that the endocytosis rates estimated for the two sister cells are significantly correlated (close to the $K_{endo}1 = K_{endo}2$ line (blue), $R^2=0.524$, $p=0.006$). (c) A typical filmstrip from a FRAP-TIRF experiment on CHO-Dll1-ΔICD-mCherry. Photobleached region is indicated by arrow. Scale-bar (blue) - $10\mu\text{m}$. (d) A histogram showing the distribution of endocytosis rates, K_{endo} , of CHO-Dll1-ΔICD-mCherry cells measured in 32 different cells. The average endocytosis rate is $K_{endo} = 0.019\text{s}^{-1}$ with standard deviation of 0.012s^{-1} . This distribution is not significantly different than the distribution of the full cell population in Fig. S1a ($p=0.855$ as calculated by Wilcoxon rank-sum test). (e) Calculated endocytosis rates are uncorrelated with diffusion coefficients values in OCD-Dll1-mCherry cells ($R^2=-0.3$, $p=0.15$). Each point in the plot comes from a fit performed on one cell. Error bars shown correspond to the 95% confidence interval on the fitting parameters. (f) Dll1-mCherry cells subjected to $0.2\mu\text{M}$ Latrunculin B (or DMSO in the control) for 2 hours show disrupted acting cytoskeleton (green) but normal Dll1-mCherry distribution (red) and (g) A histogram of the diffusion coefficients, D , measured in 69 CHO-Dll1-mCherry cells. We observe a broad distribution of diffusion coefficients with average $D= 0.041\mu\text{m}^2\text{s}^{-1}$ and standard deviation of $0.041\mu\text{m}^2\text{s}^{-1}$.

Figure S3. Analysis of model parameters. Related to Fig. 3 (a) Calculated concentration profiles of free Notch (blue) and free Delta(red) for different level of expression of Delta. Here, all parameters are similar to the ones in Fig. 3c except that the exocytosis rates are taken to be $Dl_0K_{exo} = 0.2, 2, 20 [\text{a.u.}]$ in the upper, middle, and lower panels, respectively. The Notch exocytosis rate is constant in all three panels, $N_0K_{exo} = 2[\text{a.u.}]$. The concentration for all variables is normalized by the Notch concentration far from the boundary. (b) A plot showing the calculated concentration profiles of free Notch (blue) and free Delta(red) for different values of diffusion length scales. These concentration profiles become broader as the diffusion length scale increases (broadening of the Notch profile is not observed at this scale). The diffusion length scale

is defined by $\equiv \sqrt{\frac{D}{K_{endo}}}$. Calculation was performed based on the model, described in details in the supplementary text, with parameter values: $k^+ = 0.167\mu m^2 s^{-1}$, $k^- = 0.034 s^{-1}$, $k_S = 0.34 s^{-1}$, $D = 0.005, 0.16, 1 \mu m^2 s^{-1}$, $K_{endo} = 0.02 s^{-1}$, $Dl_0 K_{exo} = 0.2 \mu m^{-2} s^{-1}$, $N_0 K_{exo} = 2 \mu m^{-2} s^{-1}$, $b = 3 \mu m$. (c) A plot showing the effect of varying the diffusion coefficient of the Notch-Delta complex. Parameter values are similar to the ones in Fig. 3c except the values of $D_{[NDI]}$ (as indicated). Total signal between cells in the high (solid green line) and low (dashed green line) diffusion rates are the same within the calculation error. This shows that the diffusion of the complex can affect its distribution but not the distribution of the free Notch and Delta. (d) 5 plots showing the concentration profiles of free Delta (Dl) for different ratio of complex forming ($k^+ N_{ss}$) to endocytosis rates (K_{endo}). We look at the dependence of complex profiles as a function of the non-dimensional ratios, defined by $\alpha = \frac{k^+ N_{ss}}{K_{endo}} = \frac{\text{rate of complex forming}}{\text{rate of endocytosis}}$.

Note that $N_{ss} = \frac{k_{exo} N_0}{k_{endo}}$ (see methods). (e) 25 plots that shows the concentration profiles of total Delta ($Dl_{total} = Dl + [NDI]$) for different ratios of complex forming ($k^+ N_{ss}$), complex processing ($k^- + k^S$), and endocytosis rates (K_{endo}). We look at the dependence of complex profiles as a function of two non-dimensional ratios, α (defined in (d)), and $\beta = \frac{k^+ N_{ss}}{k^- + k^S} = \frac{\text{rate of complex forming}}{\text{rate of complex processing}}$. Here, α is the same for all the plots in the same row and β is the same for all the plots in the same columns. These plots map the behavior of the concentration profile of total Delta that can be obtained in our model. Calculation performed based on the model, described in details in the supplementary methods, with parameter values:

$$k^+ = 0.167\mu m^2 s^{-1}, k^- = 0.034 s^{-1}, D = 0.02 \mu m^2 s^{-1}, Dl_0 K_{exo} = 0.2 \mu m^{-2} s^{-1}, N_0 K_{exo} = 2 \mu m^{-2} s^{-1}, b = 3 \mu m, \alpha = \frac{k^+ N_{ss}}{K_{endo}} = 0.10, 2.57, 5.05, 7.52, 10.00 [\text{a.u.}], \beta = \frac{k^+ N_{ss}}{k^- + k^S} = 0.10, 2.57, 5.05, 7.52, 10.00 [\text{a.u.}]$$

Figure S4. Distribution of diffusion length scales of MDCK-DII1-mCherry and CHO-DII1-ΔICD-mCherry cells. Related to Fig. 4 (a) A histogram showing the distribution of diffusion length scales, λ , for MDCK-DII1-mCherry measured in 83 different cells. The distribution has a mean value $\lambda = 1.66 \mu m$ and standard deviation of $0.66 \mu m$ (same cells as Fig. S1c-e). (b) A histogram showing the distribution of diffusion length scales, λ , for CHO-DII1-ΔICD-mCherry measured in 32 different cells. The distribution has a mean value $\lambda = 0.71 \mu m$ and standard deviation of $0.54 \mu m$ (same cells as Figs. 2f, S2d-e).

Table S1. Mathematical model parameters, related to figures 3c-d, 4c, and S3b-e. A list of the parameters used to generate figures in the text and the supplementary. See discussion on choice of parameter values in the supplementary methods.

Supplemental movie captions

Movie S1. A time-lapse movie showing a typical FRAP-TIRF experiment on CHO-DII1-mCherry cells, related to Fig. 1a. The first two frames were taken prior to photobleaching and the rest of the frames were taken post-photobleaching. Time interval between frames is 0.5 sec.

Movie S2. A time-lapse movie showing a FRAP-TIRF experiment on two CHO-DII1-mCherry cells exhibiting different recovery times, related to Fig. 1d. The first two frames were taken prior to photobleaching and the rest of the frames were taken post-photobleaching. Time interval between frames is 0.35 sec.

Movie S3. A time-lapse movie showing a FRAP-TIRF experiment with two photobleached stripes in the same cell showing similar recovery times, related to Fig. 2a. The first two frames were taken prior to photobleaching and the rest of the frames were taken post-photobleaching. Time interval between frames is 0.35 sec.

Movie S4. A time-lapse movie showing a FRAP-TIRF experiment on filopodia extended from CHO-DII1-mCherry cell, related to Fig. 2d. The first two frames were taken prior to photobleaching and the rest of the frames were taken post-photobleaching. Time interval between frames is 0.35 sec.

Supplemental experimental methods

Image analysis

All data processing was performed off-line using a commercial software package (MATLAB 2014A, The MathWorks Inc., Natick, MA, 2000).

Preparation of fluorescence profiles for the movies

We have written a semi-automatic analysis code for FRAP data extraction and fitting procedure. The input of the code is a FRAP movie and the output are the fit parameters. For convenience we define below the X-axis to be along the bleached stripe and the Y-axis perpendicular to the bleached stripe (see inset in Fig 1b). The following procedure was performed:

1. *Selecting region of interest:* The general field of view (FOV) in which FRAP was performed was chose manually in the first post-bleach frame.
2. *Defining region for automated analysis:* A matlab code was written to define five rectangles centered around the bleached stripe with the same width in the X-axis ($3.9 \mu\text{m}$) and with increasing heights in the Y-axis, ($6.5/5.8/5.2/4.5/3.9 \mu\text{m}$). These 5 rectangles with different lengths are defined since different lengths may be more suitable for different profiles (see section 5 below).
3. *Background and photobleaching correction:* Camera background was subtracted from all images. Photobleaching correction (photobleaching due to continuous imaging after FRAP) was calculated by measuring the decay in fluorescence from four rectangles located $\sim 4 \mu\text{m}$ away from the FRAP area in different directions. The average decay rate α observed from these four regions was used to compensate for photobleaching, when its calculated from $\frac{F(t)}{F(0)} = 1 - \alpha t$, where $F()$ is the average fluorescence in the region as a function of time t .
4. *Averaging fluorescence along X-axis and normalizing:* To get a less noisy bleach profile, the fluorescence of each rectangle along the X-axis was averaged reducing the fluorescence data from each time point to a 1D fluorescence profile. Each post-bleach time point was then normalized by the 1D pre-bleach fluorescence profile from the same movie. 1D fluorescent profiles were rotated to correct for any tilt in the data (i.e. if one side is higher than the other side).
5. *Resulting data structure and choosing the best rectangle:* After stages 1-4 the data from each movie contain five 1D fluorescent profiles for each frame, corresponding to the five rectangles defined in stage 1. At this stage the data was manually scanned to determine the maximal rectangle size that can be used for each profile. This stage was necessary since sample noise (such as vesicles

drifting into rectangle) may affect the data quality. In any case we only used fluorescence data which was wide enough for the fluorescence to reach steady state levels.

Fitting the fluorescence profiles

6. *Fitting the first post-bleach profile:* The functions fitted to the profile are based on the functions used by (Goehring et al., 2010). In brief, we first fit the first post bleach image to:

$$A \left\{ 1 - \frac{f_b}{2} \left[\operatorname{erf} \left(m \left(\frac{d_y}{2} - y \right) \right) + \operatorname{erf} \left(m \left(\frac{d_y}{2} + y \right) \right) \right] \right\}$$

Where A is the steady state fluorescence far from the bleach center; d_y is the extent of the bleach region; m is the steepness of the boundaries of the bleach area; and f_b is the fraction that was bleached. We use Matlab's least square fit to obtain d_y , m and f_b

7. *Fitting to the whole profile:* We use the values of d_y , m and f_b obtained in step 6 to fit all the profiles in the movie to:

$$A \left\{ 1 - \frac{f_b}{2} e^{-K_{endo} t} \left[\operatorname{erf} \left(m \frac{\frac{d_y}{2} - y}{\sqrt{4Dm^2t + 1}} \right) + \operatorname{erf} \left(m \frac{\frac{d_y}{2} - y}{\sqrt{4Dm^2t + 1}} \right) \right] \right\}$$

where the two fitting parameters are the diffusion coefficient, D , and the endocytosis rate, K_{endo} , and the denoted error is the 95% confidence interval on the fitting parameters.

Unlike the description in (Goehring et al., 2010), we bleached a rectangle and not a square (as described before at 'Preparation of fluorescence profiles for the movies' section). That allows us to average over 30 pixels wide stripes and so reduce the noise. Since we extract both rates from a single FRAP measurement, we have an inherent limitation in extracting reliable endocytosis rates when the typical endocytosis times (given by $1/k_{endo}$) are much longer than typical diffusion times (given by a^2/D where a is the width of the bleach area) (Goehring et al., 2010). We estimate that this regime is likely to be relevant for diffusion coefficients of $0.1 \mu\text{m}^2/\text{sec}$ or higher.

Analysis of FRAP on filopodia

FRAP Analysis on filopodia was performed as above with the following changes:

1. Fluorescence was not averaged over x-axis (perpendicular to the filopodia). Instead maximum fluorescence was taken.
2. To take into account that no endocytosis occurs in filopodia, the value of K_{endo} was set to zero.

Mathematical model

In our model we consider a simple case in which one Notch cell attaches to one Delta cell (Figs. 3a-b). As described in the methods, we consider three main processes: (1) Notch receptors (N) and Delta ligands (Dl), exocytose into the cell membrane, in their respective cells from a large cytoplasmic pool (N_0 and Dl_0 , assumed to be constant) with rates $k_{exo}^N N_0$ and $k_{exo}^{Dl} Dl_0$, respectively. Notch receptors and Delta ligands also endocytose back into the cytoplasmic pool with rates k_{endo}^N and k_{endo}^{Dl} , respectively. Here we assume that changes in total expression vary slowly compared to membrane-cytoplasm exchange rates. (2) Notch receptors and Delta ligands diffuse laterally on the cell membrane of their respective cells with diffusion constants of D^N and D^{Dl} . And finally, (3) Notch receptors and Delta ligands can interact at the contact area. This interaction is described by a simple Michaelis-Menten reaction where a Notch receptor on one cell can bind to Delta ligand at the boundary, forming a Notch-Delta complex($[NDl]$), with association and dissociation rates k^+ and k^- . The Notch-Delta complex can be processed at a rate, k_s to generate the signal, S , which in our case is the intracellular domain of Notch (Sprinzak et al., 2010) (Fig. 3b).

Our model includes 4 reaction diffusion equations for the concentrations of Notch receptor, Delta ligand, Notch-Delta complex, and the total signal respectively:

1. $\frac{dN}{dt} = D_N \nabla^2 N + k_{exo}^N N_0 - k_{endo}^N N + I_b(r)(k^-[NDl] - k^+NDl)$
2. $\frac{dDl}{dt} = D_{Dl} \nabla^2 Dl + k_{exo}^{Dl} Dl_0 - k_{endo}^{Dl} Dl + I_b(r)(k^-[NDl] - k^+NDl)$
3. $\frac{d[NDl]}{dt} = I_b(r)(D_{[NDl]} \nabla^2 [NDl] + k^+NDl - k^-[NDl] - k_s[NDl])$
4. $\frac{dS}{dt} = I_b(r)k_s \int [NDl] d^2r - \gamma S$

Where γ is the degradation rate of the signal S , and $I_b(r)$ is the heavyside theta function defined as:

$$5. I_b(r) = \begin{cases} 1 & \text{for } r \leq b \\ 0 & \text{elsewhere} \end{cases}$$

The total signal is obtained by integrating the signal concentration over the contact area (eq. 4). We assume that the diffusion coefficient of the Notch-Delta complex $[NDl]$ is $D_{[NDl]} = \frac{D_{DL} + D_N}{4}$.

The diffusion in eq. 1-3 is a two dimensional diffusion. To reduce the dimensionality of the equations, we consider a disk-like geometry and switch to polar coordinates (where r is the radial coordinate and θ is the angular coordinate). In this geometry the contact area is a disk with diameter b and the cell is a much larger disk with radius, R . This two-disk approximation is expected to accurately capture the two cell behavior for large R (i.e., for $R \gg b$, $\sqrt{\frac{D}{k_{endo}}}$). Since the problem is radially symmetric we can integrate the equations along the angular coordinate and reduce the equations to 1D reaction-diffusion equations. Writing the Laplacian in polar coordinates we get:

6. $\frac{dN}{dt} = D_N \left(\frac{\partial^2 N}{\partial r^2} + \frac{1}{r} \frac{\partial N}{\partial r} \right) + k_{exo}^N N_0 - k_{endo}^N N + I_b(r)(k^- [NDl] - k^+ [NDl])$
7. $\frac{dDL}{dt} = D_{DL} \left(\frac{\partial^2 DL}{\partial r^2} + \frac{1}{r} \frac{\partial DL}{\partial r} \right) + k_{exo}^{DL} DL_0 - k_{endo}^{DL} DL + I_b(r)(k^- [NDl] - k^+ [NDl])$
8. $\frac{d[NDl]}{dt} = I_b(r) \left(D_{[NDl]} \nabla^2 [NDl] + k^+ NDl - k^- [NDl] - k_S [NDl] \right)$
9. $\frac{dS}{dt} = I_b(r) k_S 2\pi \int [NDl] r dr - \gamma S$

We consider that at the edge of the cell, (at $r = R$) far enough from the contact area, there is no flow, so the boundary condition are:

$$10. \frac{\partial N}{\partial r} \Big|_{r=R} = 0$$

$$11. \frac{\partial DL}{\partial r} \Big|_{r=R} = 0$$

Simulation Parameters

For all the simulations, except of the one in Fig. 4c we considered:

$$D^N = D^{DL} = D, k_{endo}^N = k_{endo}^{DL} = k_{endo}, k_{exo}^N = k_{exo}^{DL} = k_{exo}$$

The initial level of Notch and Delta, in all the figures, is the steady state level of the non-interacting cells, defined as N_{ss} and DL_{ss} , respectively. These are calculated by solving the steady state of the equations without interactions:

$$12. \frac{dN}{dt} = D_N \nabla^2 N + k_{exo} N_0 - k_{endo} N$$

$$13. \frac{dDl}{dt} = D_{Dl} \nabla^2 Dl + k_{exo} Dl_0 - k_{endo} Dl$$

The steady state solutions are then:

$$14. N_{ss} = \frac{k_{exo} N_0}{k_{endo}}$$

$$15. Dl_{ss} = \frac{k_{exo} Dl_0}{k_{endo}}$$

Equations 6-9 were used to calculate the Figures 3c-d, 4c, S3. These figures were obtained using PDE solver of Matlab.

Parameters estimation

The parameters used in the simulations are provided in Table S1. Some of the parameters were obtained from our experimental results while others were estimated based on literature and simple dimensional analysis described below.

D and K_{endo} are obtained from our measurements (Fig. 1e, Fig. S1a).

$K_{exo} N_0, K_{exo} Dl_0$ were obtained using Eq. 14 and 15. Since the concentration range of transmembrane proteins is between $1-1000 \mu\text{m}^{-2}$ ((McCloskey and Poo, 1986) (Waters et al., 1990) (Shimizu et al., 1999)) and since we considered the case where $Dl_0 < N_0$ we chose $N_{ss} = 100 \mu\text{m}^{-2}$ and $Dl_{ss} = 10 \mu\text{m}^{-2}$. We therefore get $Dl_0 k_{exo} = 0.2 \mu\text{m}^{-2}\text{s}^{-1}$ and $N_0 k_{exo} = 2 \mu\text{m}^{-2}\text{s}^{-1}$.

To estimate $k^+, k^-,$ and k_s we started with literature values for 3D binding affinity of soluble Dll1 to Notch1, $k_{d3D} = 3.4 \mu\text{M}$ (Andrawes et al., 2013), and typical on rate for protein binding, $k^+_{3D} = 10^5 \text{M}^{-1}\text{s}^{-1}$ (Schlosshauer and Baker, 2004). Using the equilibrium relation, $k_{d3D} = \frac{k_{off}}{k^+_{3D}}$, we obtain an estimation of the off rate, $k_{off} = 0.34 \text{s}^{-1}$ for the reaction.

To switch to 2D parameters we use the relation obtained in (Wu et al., 2013), (Wu et al., 2011), $\lambda_d = \frac{k_{d2D}}{k_{d3D}}$, where λ_d is a typical length scale associated with the plasma membrane thickness which was shown to be approximately 1nm for many biological systems. After conversion of concentration from Molar to metric units, we get $k_{d2D} = 2.04 \mu\text{m}^{-2}$.

Next, we use the equilibrium relation $k_{d2D} = \frac{k_{off}}{k^+_{2D}}$ to obtain the value of the 2D on rate, $k^+_{2D} = 0.167 \mu\text{m}^2\text{s}^{-1}$ (we assume the same off rate as in 3D). Since we consider the case where $k_S \gg k^-$, we took $k_S = k_{off}$, and then take $k^- = \frac{k_S}{10}$.

References

- Andrawes, M.B., Xu, X., Liu, H., Ficarro, S.B., Marto, J.A., Aster, J.C., and Blacklow, S.C. (2013). Intrinsic selectivity of Notch 1 for Delta-like 4 over Delta-like 1. *J Biol Chem* **288**, 25477-25489.
- Goehring, N.W., Chowdhury, D., Hyman, A.A., and Grill, S.W. (2010). FRAP analysis of membrane-associated proteins: lateral diffusion and membrane-cytoplasmic exchange. *Biophys J* **99**, 2443-2452.
- McCloskey, M.A., and Poo, M.M. (1986). Rates of membrane-associated reactions: reduction of dimensionality revisited. *J Cell Biol* **102**, 88-96.
- Schlosshauer, M., and Baker, D. (2004). Realistic protein-protein association rates from a simple diffusional model neglecting long-range interactions, free energy barriers, and landscape ruggedness. *Protein Sci* **13**, 1660-1669.
- Shimizu, K., Chiba, S., Kumano, K., Hosoya, N., Takahashi, T., Kanda, Y., Hamada, Y., Yazaki, Y., and Hirai, H. (1999). Mouse jagged1 physically interacts with notch2 and other notch receptors. Assessment by quantitative methods. *J Biol Chem* **274**, 32961-32969.
- Sprinzak, D., Lakhanpal, A., Lebon, L., Santat, L.A., Fontes, M.E., Anderson, G.A., Garcia-Ojalvo, J., and Elowitz, M.B. (2010). Cis-interactions between Notch and Delta generate mutually exclusive signalling states. *Nature* **465**, 86-90.
- Waters, C.M., Oberg, K.C., Carpenter, G., and Overholser, K.A. (1990). Rate constants for binding, dissociation, and internalization of EGF: effect of receptor occupancy and ligand concentration. *Biochemistry* **29**, 3563-3569.
- Wu, Y., Honig, B., and Ben-Shaul, A. (2013). Theory and simulations of adhesion receptor dimerization on membrane surfaces. *Biophys J* **104**, 1221-1229.
- Wu, Y., Vendome, J., Shapiro, L., Ben-Shaul, A., and Honig, B. (2011). Transforming binding affinities from three dimensions to two with application to cadherin clustering. *Nature* **475**, 510-513.